

CRUSTAL STRUCTURE OF THE
CENTRAL LESSER ANTILLES ISLAND ARC:
SEISMIC NEAR-VERTICAL AND WIDE-ANGLE PROFILING

DISSERTATION
ZUR ERLANGUNG DES DOKTORGRADES
DER MATHEMATISCH-NATURWISSENSCHAFTLICHEN FAKULTÄT
DER CHRISTIAN-ALBRECHTS-UNIVERSITÄT
ZU KIEL

Wolfgang Weinzierl

Kiel, September 2010

Referent/in:

Prof. Dr. H. Kopp

Korreferent/in:

Prof. Dr. E. R. Flueh

Tag der mündlichen Prüfung:

09.07.2010

Zum Druck genehmigt:

15.09.2010

Der Dekan

Abstract

In the context of the EU funded THALES project active seismic investigations were conducted along the Lesser Antilles subduction zone, using both, wide-angle and near-vertical techniques. The structure of the Caribbean plate and the subducting Atlantic plate was determined through a combined analysis of ocean bottom seismometer and multi-channel seismic data along a transect between 15° N and 17° N. A detailed analysis of a priori and a posteriori information of a Monte Carlo based tomography scheme with a subsequent structural evaluation by forward modeling are applied to a 2-d seismic profile south of Guadeloupe.

The island arc crust of the Caribbean plate has an average thickness of 28 ± 2 km and overrides the approximately 8 km thick late cretaceous (80 Ma) Atlantic crust. The island arc crust shows two distinct reflections, which are interpreted as an intracrustal and Moho discontinuity, respectively. To a depth of 40 km the Atlantic lithosphere subducts at an average angle of 40° . The accretionary prism gains a thickness of more than 10 km and shows high energy attenuation in the middle prism. A backstop structure is imaged by a strong lateral increase of the vertical velocity gradient superimposed on structural heterogeneities. The decollement zone reaches a thickness of up to 1.8 km and shows no seismic phase polarity change.

The slow convergence rate and the subduction of the Tiburon and Barracuda ridges make this subduction zone a prime candidate for major earthquakes. Between 15° N and 17° N, the seismogenic rupture area is approximated by the contact zone between the backstop and the mantle wedge. Accordingly, this area is capable of triggering an earthquake of a magnitude of M_w 7.6 and indeed makes this active European subduction zone a place of major telluric risk.

Zusammenfassung

Im Rahmen des von der EU finanzierten THALES Projektes wurden aktive seismische Untersuchungen entlang der Antillischen Subduktionszone durchgeführt. Die kombinierte Analyse der Weit- und Steilwinkeldaten löst die Struktur der Karibischen Platte sowie der subduzierenden Atlantischen Platte zwischen 15°N und 17°N in noch nie dagewesener Genauigkeit auf. Eine umfassende Analyse der a priori und a posteriori Distributionen im Rahmen einer auf der Monte Carlo Methode basierten Tomographie mit einer anschließenden Vorwärtsmodellierung wird entlang eines seismischen 2-d Profils südlich von Guadeloupe durchgeführt.

Die Inselbogenkruste der Karibischen Platte hat eine mittlere Dicke von 28 ± 2 km und wird von der im Mittel 8 km dicken ca. 80 Ma alten Atlantischen Kruste subduziert. Innerhalb des Inselbogens konnten zwei klare Reflektoren, die als intrakrustal und Moho Diskontinuität identifiziert wurden, modelliert werden. Bis auf eine Tiefe von 40 km subduziert die Atlantische Kruste mit einem mittleren Winkel von 40° . Der Akkretionskeil erreicht eine Dicke von bis zu 10 km und weist eine sehr starke Energieabschwächung im mittleren Prisma auf. Eine in ihrer strukturellen Heterogenität einzigartige 'backstop' Struktur konnte anhand von sehr hohen lateralen Zuwächsen der vertikalen Geschwindigkeitsgradienten identifiziert werden. Die 'decollement' Zone erreicht eine Dicke von bis zu 1.8 km und weist keine Umkehrung der seismischen Phasenpolarität auf.

Die geringe Konvergenzrate sowie die Subduktion des Tiburon beziehungsweise des Barracuda Rückens machen diese Subduktionszone zu einer Region, die durch sehr starke Erdbeben erschüttert werden könnte. Zwischen 15°N und 17°N kann die seismogene Zone durch die Interplattengrenze zwischen 'backstop' und Mantelkeil

approximiert werden. Dementsprechend kann man bei dieser aktiven europäischen Subduktionszone davon ausgehen, dass ein mögliches Erdbeben der Stärke M_w 7.6 fatale Folgen für die Bevölkerung haben würde.

Contents

Abstract	ii
Zusammenfassung	iii
1 Introduction	1
1.1 Regional Tectonics	7
1.2 Statistical Separation of a Wide-Angle Profile	9
2 Monte Carlo Splitting	11
2.1 Introduction	11
2.2 Data Acquisition and Tomographic Modeling	12
2.3 Results of Monte Carlo Estimation	18
2.4 Analyzing the Backstop	23
2.5 Conclusion	30
3 Wide-Angle Modeling	32
3.1 Introduction	33
3.2 Regional Tectonic Setting And Previous Investigations	34
3.3 Data Acquisition and Processing	38
3.4 Tomographic Inversion	39
3.4.1 Combining the near-vertical and wide-angle data	42
3.5 Forward Modeling	43
3.6 Results	46
3.7 Discussion and conclusions	53

3.7.1	Oceanic Domain	53
3.7.2	Forearc-island arc transition and backstop topography	53
3.7.3	Island arc structure	55
4	Conclusions	61
4.1	Methodology	62
4.2	Geology	62
4.2.1	Seismogenic zone and rupture area	63
4.3	Outlook	65

Chapter 1

Introduction

For the past four decades, offshore geophysical observations have radically changed our view of plate interactions along convergent margins. The subduction of dense oceanic lithosphere beneath less dense continental or island arc lithosphere is capable of triggering large hazardous earthquakes along their megathrust fault planes and is dominated by accreting vs. eroding material transfer mechanisms (Von Huene and Scholl, 1991), though these may be regarded as end-member scenarios. Depending on the convergence rates and the sedimentary cover of the incoming plate, accretionary and erosive margins are distinguished by their mass flux (Clift and Vannucchi, 2004). Most margins experience alternating phases of accretion and erosion in time and space (i.e. along strike of the trench). Accretion is typically favored in regions of slow convergence rates (<6 cm/a) and trench sediment thicknesses exceeding 1 km. Figure 1.1 shows a schematic cross section of both end-member types. Although subduction erosion dominates along more than 60% of the convergent margins, the following discussion is limited to the tectonical units and processes imaged in regions of very low convergence, which create thick accretionary prisms (Von Huene and Scholl, 1991).

At the trench axis the upper plate is bordered by the frontal prism with widths from 5 km to ~ 30 km (Gutscher and Westbrook, 2009; von Huene and Ranero, 2009) (Fig. 1.2). The material composition of the frontal prism is dependant on a number of mechanical processes and is derived from off-scraped trench fill, slope apron sediments

or basement rock (Von Huene and Scholl, 1991). As the plates converge, this tectonic unit begins consolidation at the contact zone to the accreted prism and eventually becomes part of it.

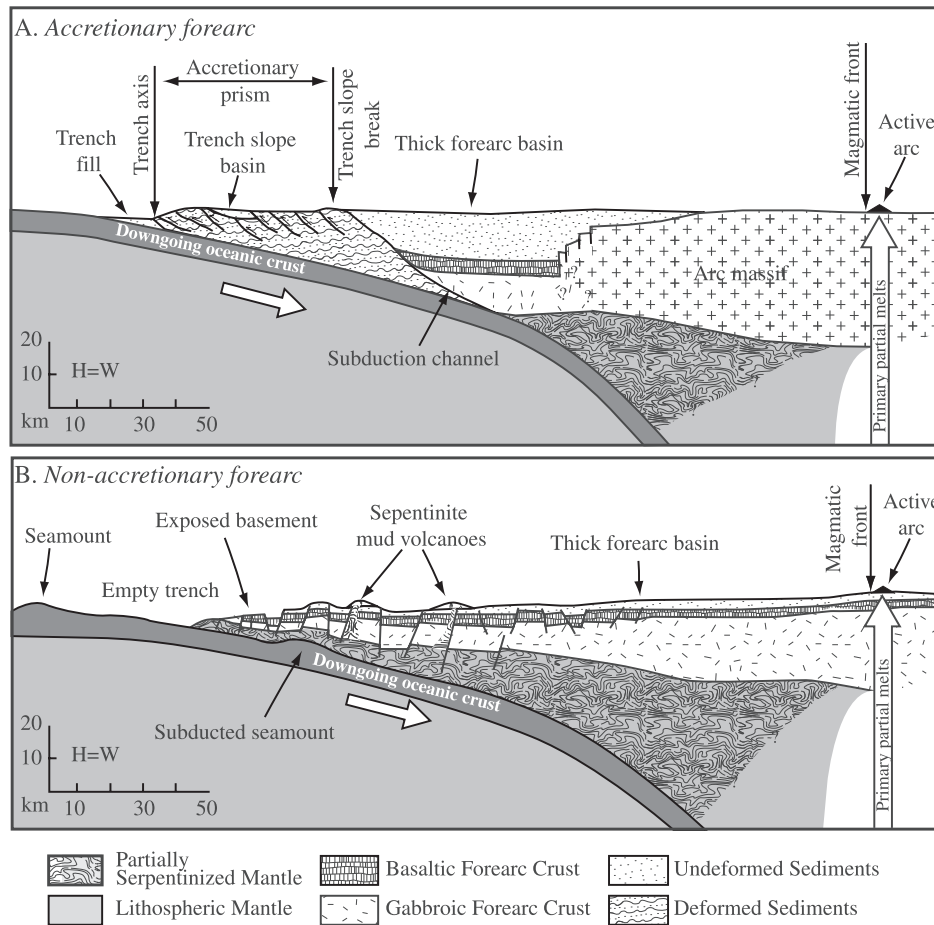


Figure 1.1: Schematic cartoon of the two basic types of margins. (A) Accretionary and (B) erosive (after Stern, 2002).

Advancing further, one enters the middle prism which is often difficult to image by near-vertical seismic acquisition, due to little deformation in the older accreted material. The middle prisms can reach widths of nearly 100 km (von Huene and Ranero, 2009) at margins bordered by thickly sedimented trenches with an orthogonal convergence of <4 cm/a. Developing from frontal prisms, the middle prism consists of consolidated and rigid sedimentary rock which ultimately enlarge a continents'

or island arcs' width. The middle prism is bound landward by the backstop (Byrne et al., 1988; Wang and Davis, 1996). Following its original definition, the backstop is a distinctive kinematic boundary at the front of the overriding plate (Byrne et al., 1988). The material it is composed of is significantly stronger, i.e. crystalline basement or consolidated sediments (Kopp and Kukowski, 2003), than the sediment lying further trenchward. This can either be seen in the higher velocities derived from wide-angle seismic data or be visualized by strong acoustic reflections on near-vertical seismic sections.

ROCK UNIT SEGMENTATION

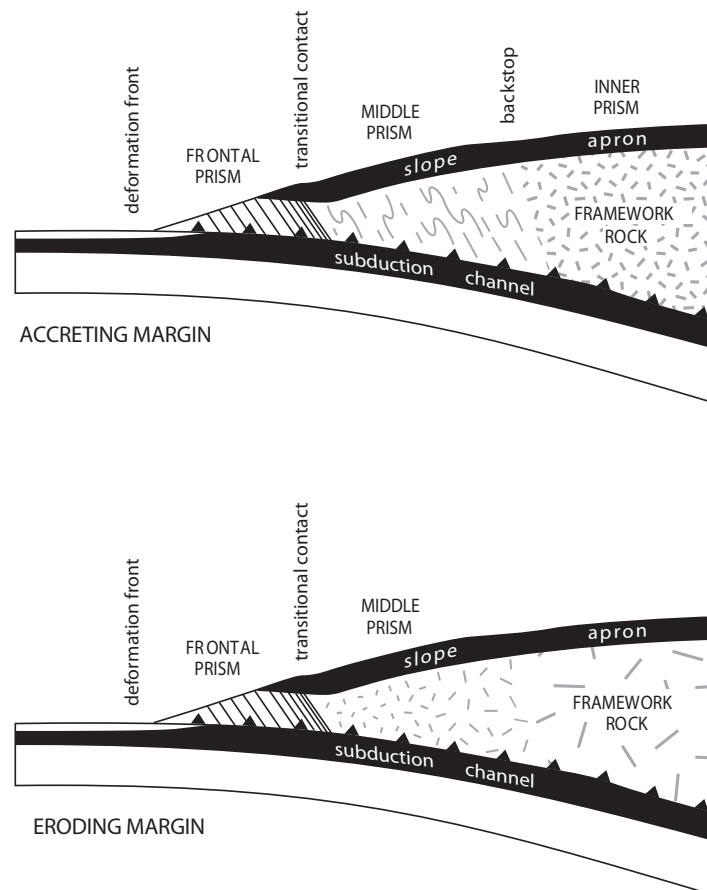


Figure 1.2: Rock and sediment framework at accretionary (top) and eroding (bottom) margins (after von Huene and Ranero, 2009).

The backstop partitions subducting sediments into the accretionary wedge or diverts them deep into the subduction zone (Bangs et al., 2003). Additionally, the backstop has been thought of controlling the updip limit of plate boundary seismicity (Byrne et al., 1988; Fuller et al., 2006). Moving further landward, one enters the forearc basin domain which is characterized by parallel - sometimes deformed - sediment sequences (Collot and Fisher, 1989). The deformation of these sequences is strongly dependant on the geomorphology of the incoming plate. Ridge as well as seamount subduction have a strong influence on their evolution (Bangs et al., 2006; Nishizawa et al., 2009). Forearc basins might have a significant influence on subduction zone earthquakes (Fuller et al., 2006) and represent a major deviation from an oversimplified wedge-shape theory for the overriding plate (Davis et al., 1983; Dahlen et al., 1984). In their numerical simulations, Fuller et al. (2006) demonstrate that the sedimentation stabilizes the underlying wedge, ultimately posing a possible telluric risk, since maximum slip associated with great-thrust earthquakes generally occurs in these areas.

Beneath the frontal and locally into the middle prism seismic images have revealed a layer which plays a dominant role in fluid cycling at the interplate contact (e.g. Bangs et al., 2003; von Huene and Ranero, 2009). The minimally deformed stratified trench fill subducting below the frontal prisms decollement becomes subject to higher pressures and temperatures while being transported in the direction of the middle prism. The fluids are drained from this subduction channel until the seismic velocities match the framework rock at the transition from aseismic to seismogenic behavior (Ranero et al., 2008).

The relevance to understand and interpret the structural evolution and composition in a subduction zone lies at hand, if one considers that the largest and most destructive earthquakes occur on subduction zone thrust faults (Byrne et al., 1988). Earthquakes nucleate as a result of stick-slip frictional instability (Brace and Byerlee, 1966; Ida, 1975). The transition from aseismic, stable sliding to seismic, stick-slip behaviour is controlled by various parameters such as temperature, pressure, and abundance of fluids (Kato and Hirasawa, 1999; Hyndman and Wang, 1993; Saffer and Marone, 2003). The knowledge of the geometry of the seismogenic zone, the part of the interplate boundary where the nucleation might occur, is therefore of utter importance

for the assessment of seismic risk.

The Lesser Antilles subduction zone and its accretionary system have been the subject of numerous seismic reflection and refraction surveys which have revealed the igneous forearc crust, accretionary wedge, backstop and forearc basin structure near 16° N (Bangs et al., 1990, 2003; Christeson et al., 2003). This subduction zone with its accretionary system is an optimal location to study the impact of the backstop structure on the interaction between the overriding arc and the subducting oceanic crust.

There are numerous reasons for this region to act as a case study on the evolution of a backstop structure. The thick accumulation of sediments in this region accompanied by the slow convergence process (Feuillet, 2000) results in a highly compacted parallel sedimentation deformed by the Tiburon and the Barracuda ridge subduction (see Fig. 1.3). Not only is this of interest to deep structure imaging, but furthermore to processes of geological timescales ultimately focussing on the actual impact on human kind, i.e. why does this region seem so aseismic? Detailed passive and active seismic observations were carried out as part of the EU funded THALES (Transients in the Hellenic and Antilles Loci of Earthquakes of European Subductions: Water Activity, Structure, and Seismic Risk Illuminated by Geophysical High-Technology) project in 2007 to assess the telluric risk in this region. One of the main goals of the work, using RV Maria S. Merian and RV Atalante, was the mapping of the location, size, and spatial variation of the potentially seismogenic megathrust fault on the Antilles subduction interplate boundary. This thesis presents the results of a 2-D seismic wide-angle profile acquired in the Lesser Antilles. The transect is one of a few which crosses a complete island arc (Kodaira et al., 2008; Takahashi et al., 2009) and gives insights to the continental crust evolution of the Caribbean plate and the contact zone with the subducting North American plate.

In general, an ideal seismic experiment will comprise both, near-vertical incidence and dense wide-angle profiling, to permit the best possible velocity determination and accurate imaging through prestack depth migration since both approaches have limitations if handled independently. Velocity models derived from wide-angle data lack the detail that imaging by migration can provide because only a small subset

of the recorded wave field is used. On the other hand, near-vertical incidence data does not constrain deep-crustal velocities necessary for depth migration. The data acquired during the cruises of RV Maria S. Merian and RV Atalante consisted of both, wide-angle and near-vertical data, respectively.

This thesis focusses on two scientific aspects: a statistical approach to data analysis and a neotectonic interpretation of structural information obtained from ocean bottom seismometer (OBS) and multi-channel seismic (MCS) data. Chapter I presents the regional framework and introduces the motivation of the methods used to analyze the 2-D profile. Chapter 2 defines the inverse problem emphasizing its non-unique character. It further explains the methodology used to retrieve the backstop structure and provides the foundation for the wide-angle modeling of later arrivals presented in Chapter 3. With a mean velocity field revealed by the tomographic study, the structural image of the backstop, and the secondary arrivals seen in the seismic sections, it is possible to construct a deep structural image of the subduction zone complex of our profile as demonstrated in Chapter 3. Implementing the results of the tomographic study, I construct a forward model for this complex subduction zone. This is of great interest for passive studies since it gives a more detailed structural composition for locating earthquakes. MCS data obtained on a part of the presented transect serves as a-priori information for defining deeper structures. Chapter 2 and 3 have been written in manuscript form. Chapter 2 is in press in *Geophysics* and Chapter 3 is currently being submitted to *Earth and Planetary Science Letters*.

In order to comprehensively understand this subduction zone complex and to meet the key objectives of this project, the assessment of the structural composition of a 2-D profile across the complete island arc, is essential. The structural model reveals the igneous forearc, the accretionary prism, the backstop and the subducting Atlantic crust south of Guadeloupe. The central island arc is imaged for the first time by means of wide-angle seismic data and the model reveals the structural complexity of this subduction zone.

1.1 Regional Tectonics

The Lesser Antilles arc is a ~ 850 km long island arc formed by the subduction of the Atlantic seafloor under the Caribbean plate (see Fig. 1.3). The Caribbean plate is bounded to the North and to the South by two systems of strike-slip faults (Adamek et al., 1988; Flinch et al., 1999; Heubeck and Mann, 1991; Holcombe et al., 1990; Mann et al., 1995; Jordan, 1975; Mascle and Letouzey, 1990; Weber et al., 2001) with a strongly curved subduction zone in between forming its eastern boundary. This subduction zone absorbs the ENE motion between the American and the Caribbean plates, that converge at a rate of ~ 2 cm/a. The island arc is situated around 200 km to 400 km parallel to the west of the trench. Its history is rather complex and two main volcanic fronts can be identified (Bouysse, 1988). An early Eocene volcanism constitutes the older arc, whereas the recent and still active arc, settled several million years after the older arc ceased its activity. South of Martinique, the recent volcanism re-occupied the same position as the older arc. However, from Martinique northwards, the recent arc is offset progressively from the older one to the west. As a result of this, the eastern (Grande Terre) and western (Basse Terre) parts of the island of Guadeloupe are of different volcanic origin. This separation of the recent and older arcs is proposed to be the result of kinematic changes in the subduction processes (Bouysse and Westercamp, 1990). The trench of the subduction is filled mainly with sediments coming from South American rivers, such as the Amazon and Orinoco. The consequence of this huge sedimentary input is the presence of an important sedimentary prism. The accretionary prism width increases towards the south and shows a maximum thickness of 20 km (Westbrook, 1975, 1982) at the Barbados accretionary prism. A strong negative magnetic anomaly (Bowin, 1976), observed ~ 150 km east of the present volcanic front, indicates the location of the contact between the Caribbean and the subducted Atlantic crust. This subduction zone is characterized by a slow convergence rate (~ 2 cm/a) and the subduction of a relatively old oceanic crust (Lower Campanian-Maestrichtian). Another characteristic of the subducting plate is the presence of several fracture zones initiated at the Mid-Atlantic ridge. Three WNW-trending ridges of the Atlantic oceanic crust are

presently being subducted beneath the Lesser Antilles.

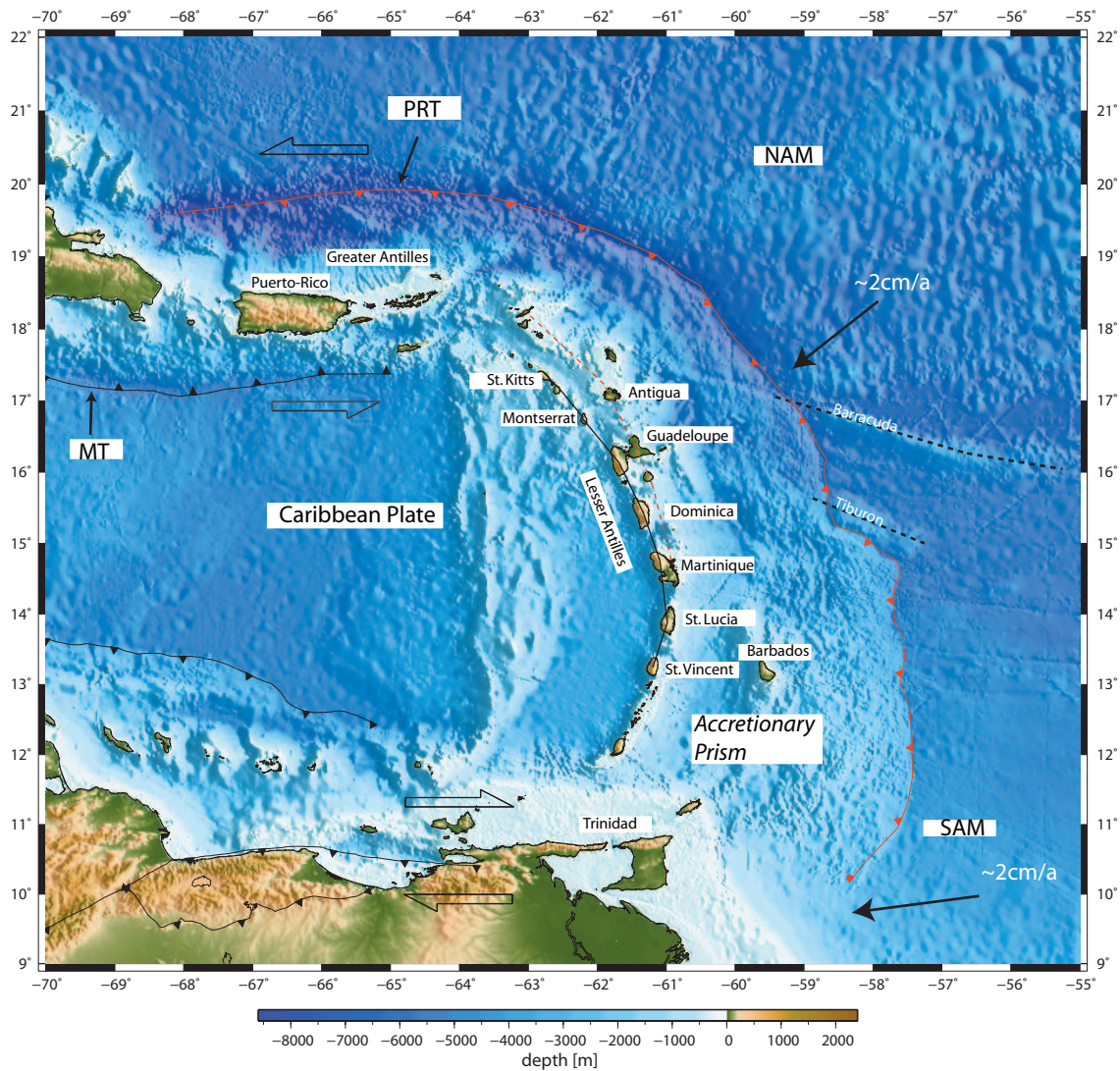


Figure 1.3: Tectonic setting of the Lesser Antilles island arc. Plate motion directions and velocities after Feuillet (2000). MT: Muertos trough, PRT: Puerto Rico trench, NAM: North American Plate, SAM: South American Plate; continuous black line, recent volcanic arc; dashed red line, ancient volcanic arc.

The 450 km long and 30-50 km wide Barracuda ridge and the 150 km long and 30-40 km wide Tiburon ridge have a bathymetric expression seaward of the Barbados

accretionary complex. They are gravimetrically uncompensated (Bouysse and Westercamp, 1990) and interpreted as fracture zones related to the segmentation of the mid-Atlantic spreading centre. Towards the South, the St. Lucia ridge is buried beneath a blanket of sediments but has been recognized by seismic reflection data. The interaction of these Atlantic bathymetric features with the leading plate margin has induced a series of effects on the evolution of the island arc. The frontal collision of the ridges faced by arc crust may produce horizontal compression, a change in the topography of the contact between the two lithospheric plates (interplate contact), and possibly a change in coupling between the plates. Another particularity of this region is the presence of the limit between the North American plate and the South American plate. First, the Barracuda ridge was thought to be the boundary (Bowin, 1976). Later, Bouysse and Westercamp (1990) proposed a diffuse boundary as large as the Lesser Antilles arc. Recently, GPS measurements (DeMets et al., 2000) and mapping of active faults (Feuillet et al., 2002) at sea show a deformation north of 16° N, with a trench parallel component of sinistral shear that decreases from ~ 15 to ~ 4 mm/yr south-eastward, seaward of Guadeloupe. South of Guadeloupe, using the South American/Caribbean plate motion vector (Weber et al., 2001), no slip partitioning exists in the southern part of the arc, consistent with the vanishing of the observed sinistral slip partitioning (Feuillet et al., 2002).

1.2 Statistical Separation of a Wide-Angle Profile

Inversion of seismic data has proven to be powerful tool to gain information on the subsurface on a regional scale and has evolved as a standard procedure in crustal structure studies. General solutions of inverse problems can often be obtained through the introduction of probability distributions to sample the model space. I present a simple approach of defining an a priori space in a tomographic study and retrieve the velocity-depth posterior distribution by using a Monte Carlo method in Chapter 2. Utilizing a fitting routine designed for very low statistics to setup and analyze the obtained tomography results, it is possible to statistically separate the velocity-depth model space derived from the inversion of seismic refraction data. The effectiveness of

this approach is demonstrated on the profile acquired in the Lesser Antilles subduction zone. The resolution analysis of the structural heterogeneity includes a divergence analysis, which proves to be capable of dissecting long wide-angle profiles for deep crust and upper mantle studies. The complete information of any parametrized physical system is contained in the a posteriori distribution. Methods for analyzing and displaying key properties of the a posteriori distributions of highly nonlinear inverse problems are therefore essential in the context of any interpretation. It is possible to map velocity variations in their extent and structure by measuring the total as well as relative divergence of the velocity structure in the a posteriori space. I apply the divergence analysis to a part of the transect where a backstop structure has been identified to show that it is capable of resolving shallow features while returning some information concerning the confidence level of results. Under the assumption of a relationship between forearc and backstop, a structural image in accordance with previous interpretations is obtained.

Chapter 2

Monte Carlo Splitting

2.1 Introduction

Numerous studies dealing with inverse problems have been approached in as many ways as there are questions to be answered by them (Parker (1994)). The theory of seeking parameters by indirect measurements has been applied successfully by Parker and Dziewonski (1995) in a more phenomenological fashion than the one Hjelt (1992) chose by inference in a more qualitative way or the rigorous mathematical approach of Kirsch (1996). The re-formulation of the theory in a non-parametric fashion has enabled a statistical approach and error analysis to quantitatively evaluate and investigate the solutions to any inverse problem. In this Bayesian formulation the most general solution of any inverse problem is a probability distribution of the model space. Analytic techniques solving this problem are only applicable in the simplest case, i.e. only one global minimum and no local minima exist. Since this ideal case is almost never met, extensive exploration of the model space has to be performed. There have been numerous examples of solutions to inverse problems by means of Monte Carlo methods (e.g., Press (1968), Press (1971), Mosegaard and Tarantola (1995), Jacobsen et al. (1996b), Jacobsen et al. (1996a), Mosegaard and Sambridge (2002), Sambridge and Mosegaard (2002)). A major concern in this Bayesian approach is the knowledge of an a priori distribution for the setup of starting models to sample the model space (Hansen et al. (2006)). One way of simplifying and reducing such a search to a limited

band of models for inversion is the introduction of envelopes for parameter estimates. An uncomfortable difficulty of this approach is the inconclusive knowledge of sampling the complete model space since we are introducing boundary conditions on the p-wave-velocities in depth (Sato and Kennett (2000)). By expanding or broadening the envelopes we can expand the a priori distributions and decrease the effects of the boundary conditions.

We present a statistical separation strategy to explore the velocity-depth model space derived from the inversion of seismic refraction data. After an initial tomography with a simple 1-D velocity setup hanging below the seafloor we separate the transect according to its assumed tectonic units, namely their velocity-depth distribution. Fitting the velocity depth distributions $v(z)$ in predefined regions on the grid provides us with the essential probability density distributions for the setup of a Monte Carlo ensemble for a subsequent inversion. To test our approach we used a dataset from the Lesser Antilles margin south of Guadeloupe. The 280 km long profile traversed the island arc from the active arc region up to the accretionary prism. We invert more than 22500 first arrival travel times in over 50 starting models to enhance the statistical resolution of the final average model. The advantages of the Monte Carlo method become even more apparent in the subsequent resolution analysis. We use the total as well as relative divergence of the velocity structure of the a posteriori information to map velocity variations in their extent and structure.

2.2 Data Acquisition and Tomographic Modeling

We inverted first arrival data from a marine transect acquired with RV Maria S. Merian, cruise 4 leg 2 (MSM04/2) in 2007 in the Lesser Antilles subduction zone (see Figure 2.1). The profile was shot with a 5-element seismic source array with a volume of 112 l and a trigger interval of 60 s at a ship speed of 3.7 kn on average, resulting in a shot spacing of approximately 100 m. 44 ocean bottom seismometer (OBS) receivers were positioned at 5 km spacing along the profile. The 280 km long profile traverses the island arc and ends 70 km SE of the trench on the accretionary prism. Standard processing of the OBS data included clock drift correction, relocalization,

deconvolution, and filtering. Signal-to-noise ratios vary considerably and clear arrivals on some stations could be traced to 100-130 km offsets while the transmitted energy decreased rapidly entering the accretionary complex where first arrivals could be identified up to 20 km offsets on average.

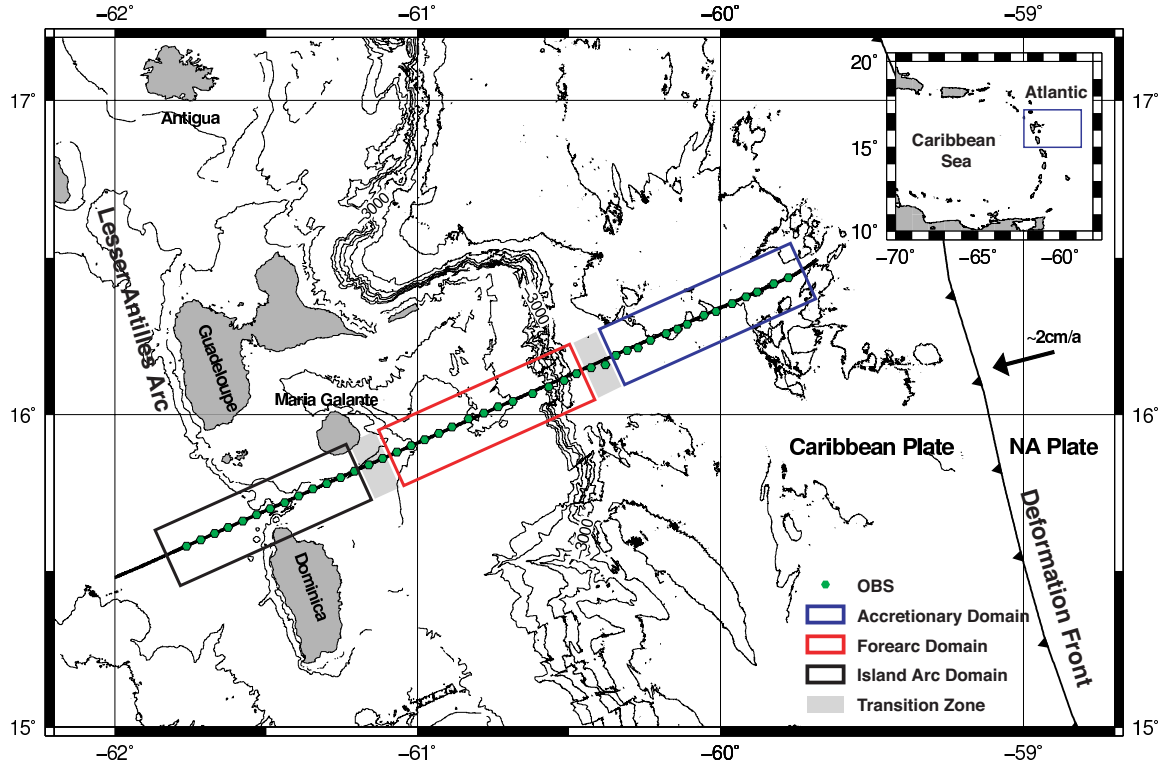


Figure 2.1: Location map of the survey site showing the deformation front between the North American (NA) and Caribbean plates. The presented profile P02 of cruise MSM04/2 of the German RV Maria S. Merian was shot at 100 m spacing and a station separation of 5 km. Circles denote relocated positions of the seismic instruments. The color coding of the transect boxes refers to the subsequent data analysis and approximately defines the arc (black), forearc (red), and accretionary (blue) regions. Inset shows regional map of the Lesser Antilles.

An initial two-dimensional velocity-depth model along the transect was obtained using the tomographic inversion method of Korenaga et al. (2000). The velocity field $v_{ik} =$

$v(x_i, z_k)$ is parametrized by a homogeneous grid of nodes with $1 \leq i \leq n_x$ and $1 \leq k \leq n_z$ below the seafloor. The matrix equation

$$\mathbf{d}_{\text{th}} = G\delta\mathbf{m} \quad (2.1)$$

with \mathbf{d}_{th} being the travel time residual vector, G the Frechet derivative matrix and $\delta\mathbf{m}$ an unknown model perturbation forms the basis of this travel time tomography. This linearized inversion procedure has been adopted from Toomey et al. (1994) and is applied iteratively until the model converges. The models were parametrized with a lateral nodal spacing of 0.5 km and variable vertical spacing of 0.05 km within the upper 2 km and increasing to 0.5 km at $z_{\text{max}} = 25$ km. To stabilize the inversion we used depth dependant smoothing constraints and correlation lengths. Correlation lengths from 1-5 km horizontally and 0.1-1 km vertically provide reliable results while using computationally less expensive larger smoothing constraints.

The starting model for the first tomographic inversion was a simple layered 1-D velocity model. The result of this inversion gave us an estimate of the velocity structure along the transect and provided the basis for defining three distinct geologic parts of the margin, namely the island arc (1), forearc high (2) and accretionary complex (3). The velocity distribution and segment definition are in accordance with earlier seismic refraction tomography results conducted in our study area (Christeson et al. (2003)).

The major drawback of the inversion problem is its non-uniqueness and there is a family of models that could fit the arrivals within the error range. With a total number of N_{tt} travel times with residuals \mathbf{d}_{th} as well as the observed residuals \mathbf{d}_{obs} a satisfactory model results in

$$\chi^2 = \frac{\sum_{i=1}^{N_{tt}} (d_{\text{obs}}(i)/d_{\text{th}}(i))^2}{N_{tt}} \quad (2.2)$$

of nearly one with a root-mean-square (rms) misfit close to the assumed picking error. Let \mathbf{m} denote the solution vector of realizations and $E(\mathbf{m})$ is the a posteriori expectation of \mathbf{m} (Tarantola (1987), Matarese (1993)). With $\sigma_{\mathbf{m}}(\mathbf{m})$ being the a

posteriori marginal density function we can write the a posteriori model covariance matrix C as

$$C = \int [\mathbf{m} - E(\mathbf{m})] \cdot [\mathbf{m} - E(\mathbf{m})]^T \sigma_{\mathbf{m}}(\mathbf{m}) d\mathbf{m} \quad (2.3)$$

This form of the covariance matrix can be approximated assuming that all realizations N are equally probable.

$$C \approx \frac{1}{N} \sum_{i=1}^N [\mathbf{m}_i - E(\mathbf{m})] \cdot [\mathbf{m}_i - E(\mathbf{m})]^T \quad (2.4)$$

with \mathbf{m}_i being the i -th realization of the solution vector \mathbf{m} .

At this stage we chose a Bayesian approach to identify the resolution of the outcome and analyze the a posteriori probability density in the model space. This can be expressed in form of a product (Tarantola (1987))

$$\sigma_M(\mathbf{m}) = k \rho_M(\mathbf{m}) L(\mathbf{m}) \quad (2.5)$$

where k is an appropriate normalization constant, ρ_M represents the a priori information on the model parameters, and the likelihood function $L(\mathbf{m})$ is a measure of the quality of the model \mathbf{m} in fitting the data (Mosegaard and Tarantola (1995)). To account for this non-uniqueness we fitted the velocities of the three distinct regions over a range of 40 km with Gaussian curves (Figure 2.2). The three distinct regions are expressed in terms of x_i :

$$\begin{aligned} x_1 - 20 &\leq x_i \leq x_1 + 20 \rightarrow \overline{v_{1k}} \\ x_2 - 20 &\leq x_i \leq x_2 + 20 \rightarrow \overline{v_{2k}} \\ x_3 - 20 &\leq x_i \leq x_3 + 20 \rightarrow \overline{v_{3k}} \end{aligned}$$

with the corresponding profile km $x_1 = 80$, $x_2 = 145$, and $x_3 = 260$. With equally weighted bins and an (improved) log likelihood method due to the very low statistics (40 km \cong 80 x-nodes) (James and Roos (1975), Brun and Rademakers (1997)) we were able to use the fitting parameters, namely the mean and deviation, to setup a

prior probability densities (see Figure 2.3), which ultimately were used to define a model space M . Under the assumption of laterally variable transition zones in between the three tectonic regimes we created more than 50 two-dimensional starting models $m(v_1, v_2, v_3, z) \in M$ for the inversion. A schematic overview of this setup is shown in Figure 2.4. The retrieval of the posterior distributions of the input ensemble can be summarized in two steps.

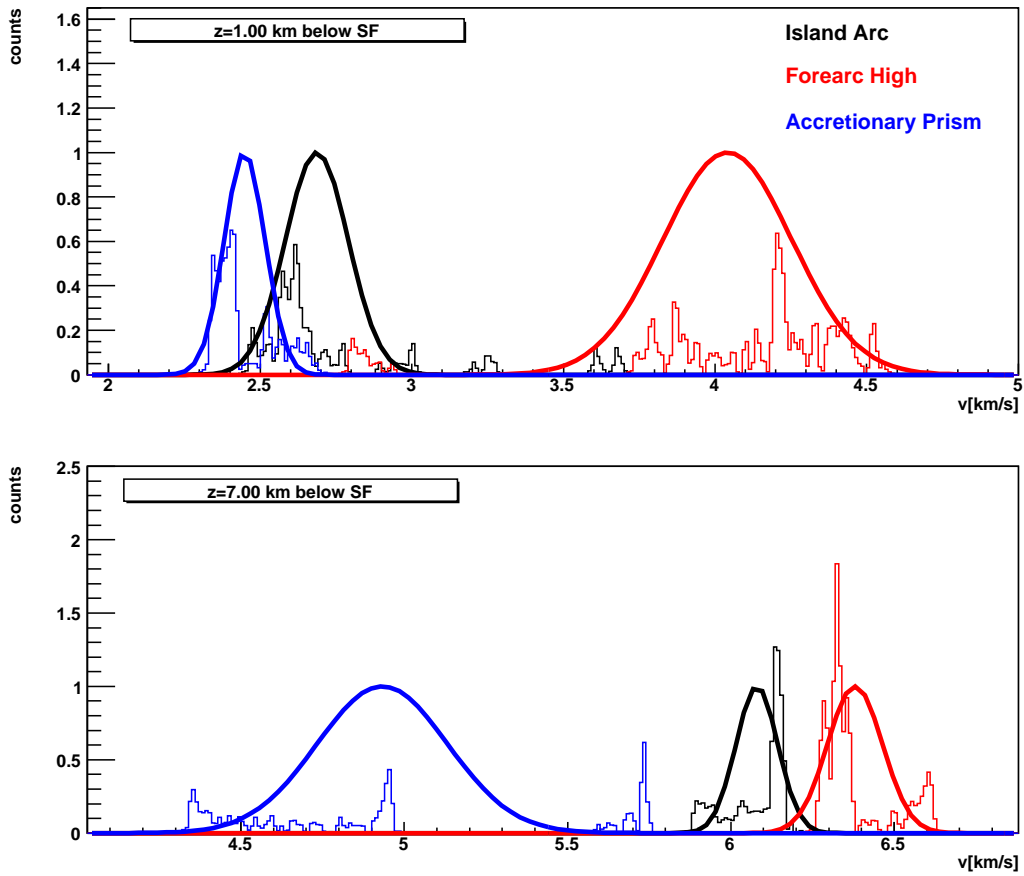


Figure 2.2: Representative fits of the velocities in the predefined regions used for the Monte Carlo estimation of 2-d initial starting models. Top panel shows the fit at $z = 1\text{km}$ and bottom for $z = 7\text{km}$ below seafloor (SF).

1. Prior input: The starting model was defined using three velocity distributions

$v_1(z)$, $v_2(z)$, and $v_3(z)$ with their corresponding confidence intervals given by the standard deviation. By linearly interpolating in between the two transition zones with variable width we constructed a two dimensional initial model for the inversion, which was completely randomized in its corresponding tectonic regions according to its confidence level.

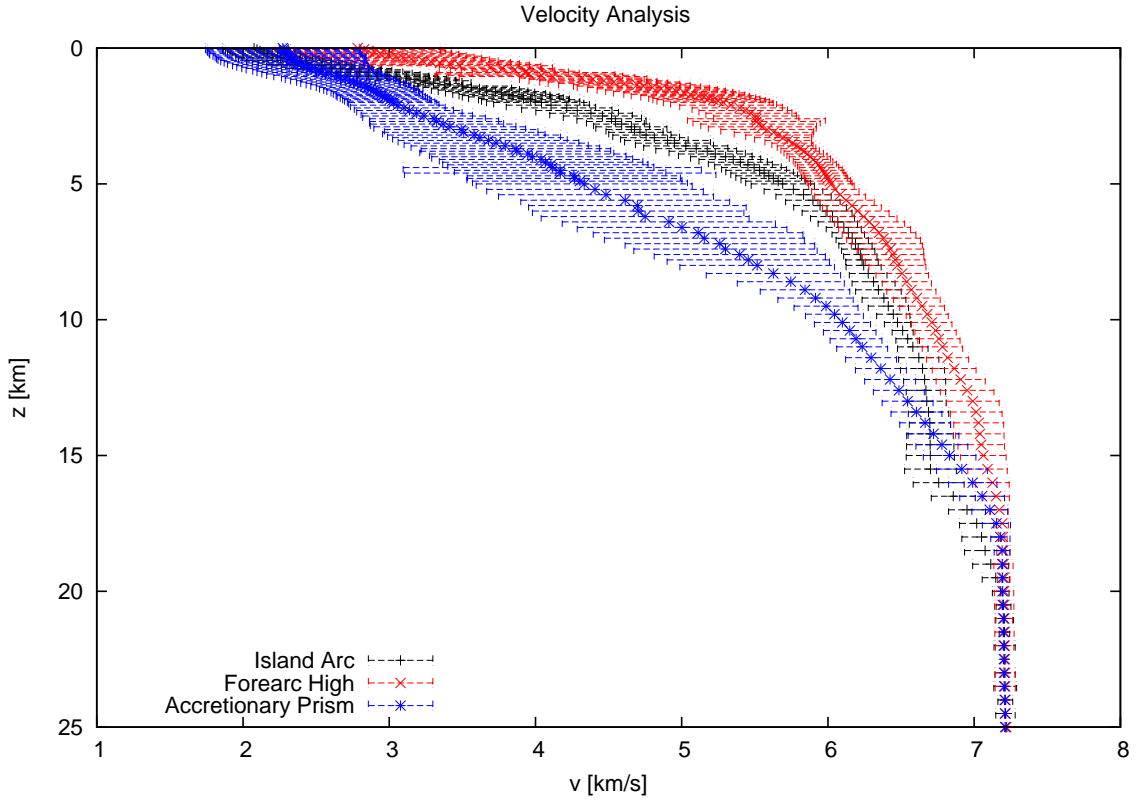


Figure 2.3: A priori velocity probability density functions used for creating two dimensional starting models. Mean values and confidence levels, recovered by the fitting procedure (Figure 2.2), define the a priori information for parameter estimation.

2. Model retrieval: Rather than doing a forward calculation to retrieve the posterior distribution through a markov chain Monte Carlo method we chose to solve the inverse problem (Tarantola (1987)) at hand with the tomographic procedure from Korenaga et al. (2000). To minimize the artifacts introduced by

large model updates we chose a top to bottom approach, increasing the number of arrivals according to the offset ranges: 0-20 km, 0-50 km and 0-130 km with spatially varying smoothing and correlation parameters.

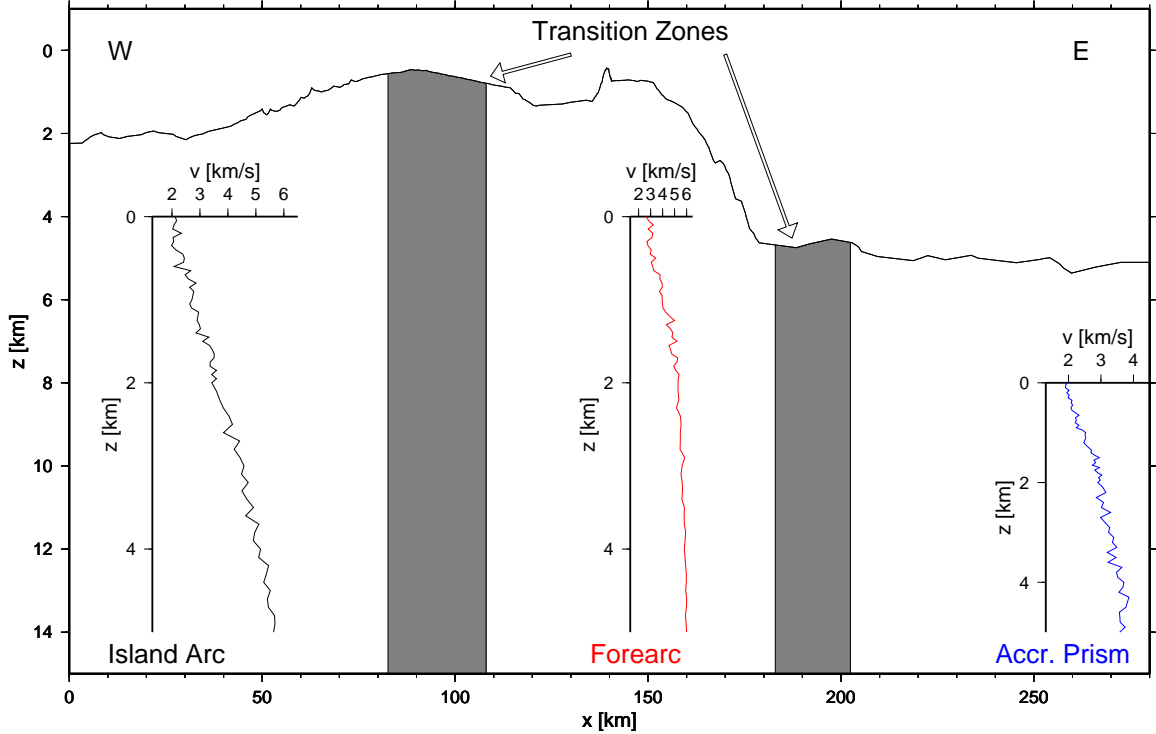


Figure 2.4: Schematic picture of model setup along the profile. Representative velocity functions used for the setup of the starting model are depicted in their color coding and the transition zones by dark gray planes in between. Seafloor bathymetry is shown by thick black line and based on swath data.

2.3 Results of Monte Carlo Estimation

The solution of any inverse problem is never one result or image but a probability distribution of samples of the posteriori probability density $\sigma(m)$ (Tarantola (1987)). The practice of calculating the mean of an ensemble of Monte Carlo realizations yields an oversimplified (smoothed) solution to the inverse problem. If a collection

of solutions is available it is possible to give a more quantitative measure for features under investigation than merely constraining the interpretation on a smoothed mean.

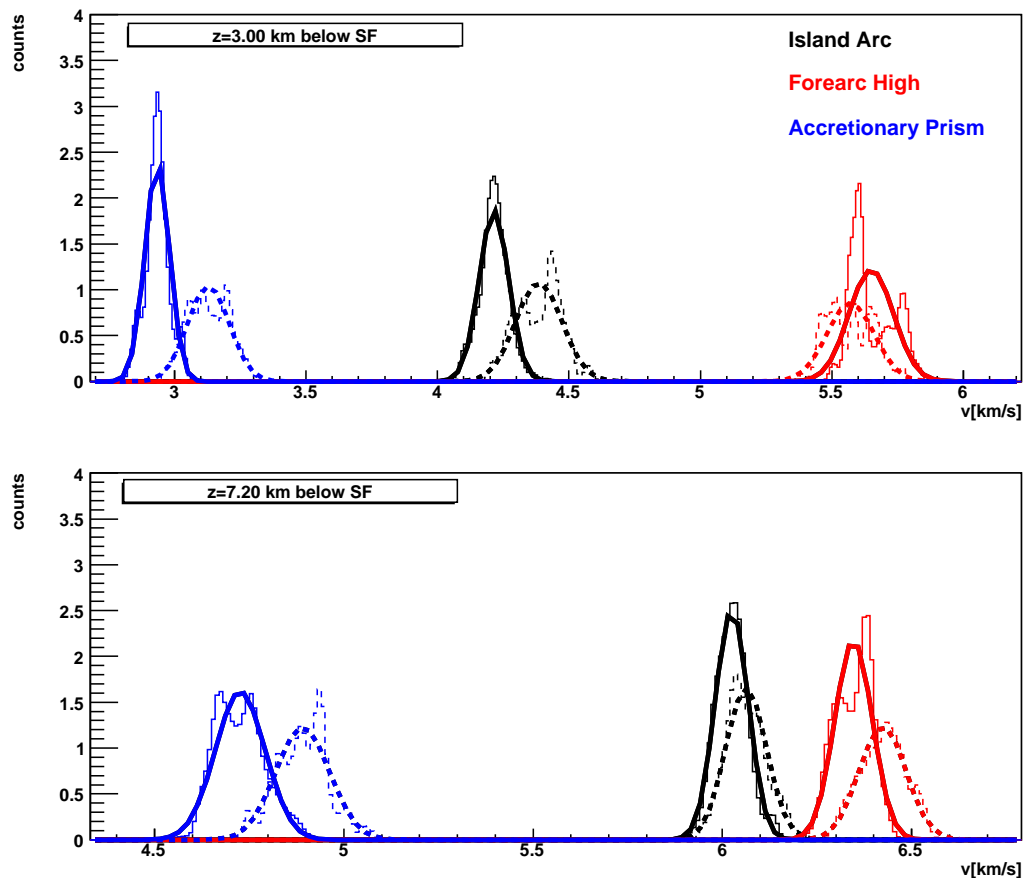


Figure 2.5: Comparison of a priori probability density (dashed) and a posteriori probability density (solid) in two representative depths below seafloor. The histograms were fitted with Gaussian curves to visualize the decrease of the variance, directly visible in the peaks and widths of the distributions, since the amount of statistics is identical. The lateral shift is due to the smoothing of the initial model before the fitting procedure to setup the 2-d models.

At this point we are able to compare the a priori with the a posteriori probability distributions (Figure 2.5). The evidence that the P-wave velocities are converging

into a minimum can be deduced from the distribution of velocities from our final Monte Carlo ensemble in comparison with our starting models. The variance of the final models is reduced and therefore velocities converge into a minimum. This test is strongly dependent on the ray coverage as can be seen in the deeper parts of the model. Only where raycoverage is sufficient we are able to increase the resolution. The actual power of the statistical approach becomes even more evident if we start analyzing the velocity structure on the basis of our initialization. Calculating the rms values Δv at each horizontal grid point (x) for each model we are able to analyze the deviations along the profile according to the mean velocity function ($\bar{v}_1, \bar{v}_2, \bar{v}_3$) used in the setup:

$$\Delta v_i(x) = \sqrt{\frac{\sum_{k=0}^{nz} (\bar{v}_i(x, z_k) - v(x, z_k))^2}{nz - 1}}, \quad i = 1, 2, 3 \quad (2.6)$$

Gaussian fitting of each distribution gives an estimate of the correlation between the mean velocity depth distributions of the distinct regions and the velocity functions along the profile. The results of this fitting procedure are shown in Figure 2.6. As expected the divergence from the mean velocity functions mimics the structural composition of the predefined tectonic regions. The divergence is smallest in the areas of highest resemblance. The transitions between these regions can be quantified by the overlap of distributions moving along the transect (Figure 2.7). Again the rms for each region is shown according to the previous color coding. The superposition of the fits and therefore total distribution is given by:

$$f_{tot}(x) = \sum_{i=1}^3 const_i e^{-0.5((\bar{dv}_i)/\sigma_i(dv))^2} \quad (2.7)$$

with $const_i$, \bar{dv}_i , and $\sigma_i(dv)$ being the normalization constant, mean, and standard deviation of the misfit to the reference distributions \bar{v}_i respectively and shown by the dashed green line in Figure 2.7.

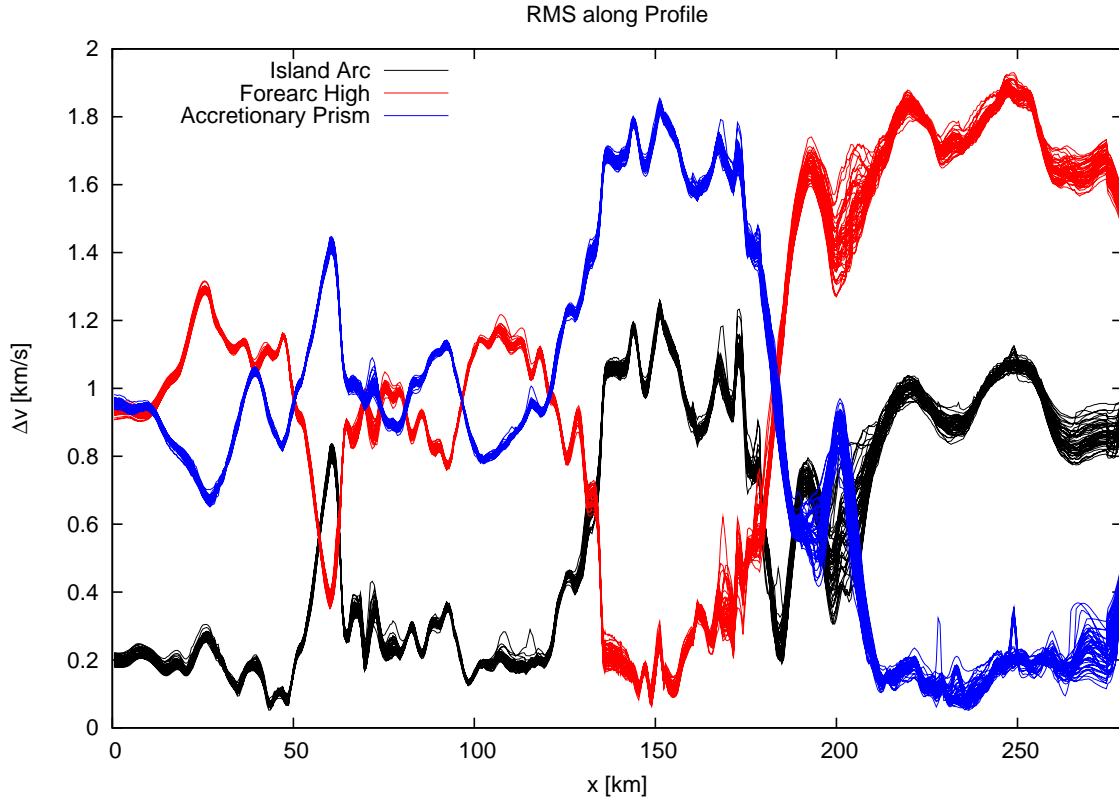


Figure 2.6: Divergence Δv_i with $i=1$ (black), $i=2$ (red), and $i=3$ (blue) along the profile. The divergence of each of the models of the resulting monte carlo ensemble was calculated according to equation 2.6.

The value of equation 2.6 is measuring the resemblance or divergence, whereas equation 2.7 is measuring the mixing ratio between the given distributions. The validity of dissecting the profile according to significant velocity depth distributions and comparing the expected distributions with the deduced velocity field can be seen around profile km 60 (Figure 2.6). The resemblance to the forearc high function is much higher since we see an increase in seismic velocities close to the seabed.

Between km 120-140 we see a fairly abrupt change in the match to Δv_1 and Δv_2 (Figure 2.6). This coincides with the transition zone between the forearc high and island arc region. Moving along the transect the divergence to the forearc high distribution Δv_2 starts increasing from profile km 165 until it enters the accretionary complex where it reaches the highest value of divergence. The distance between profile km

170-210 is not clearly

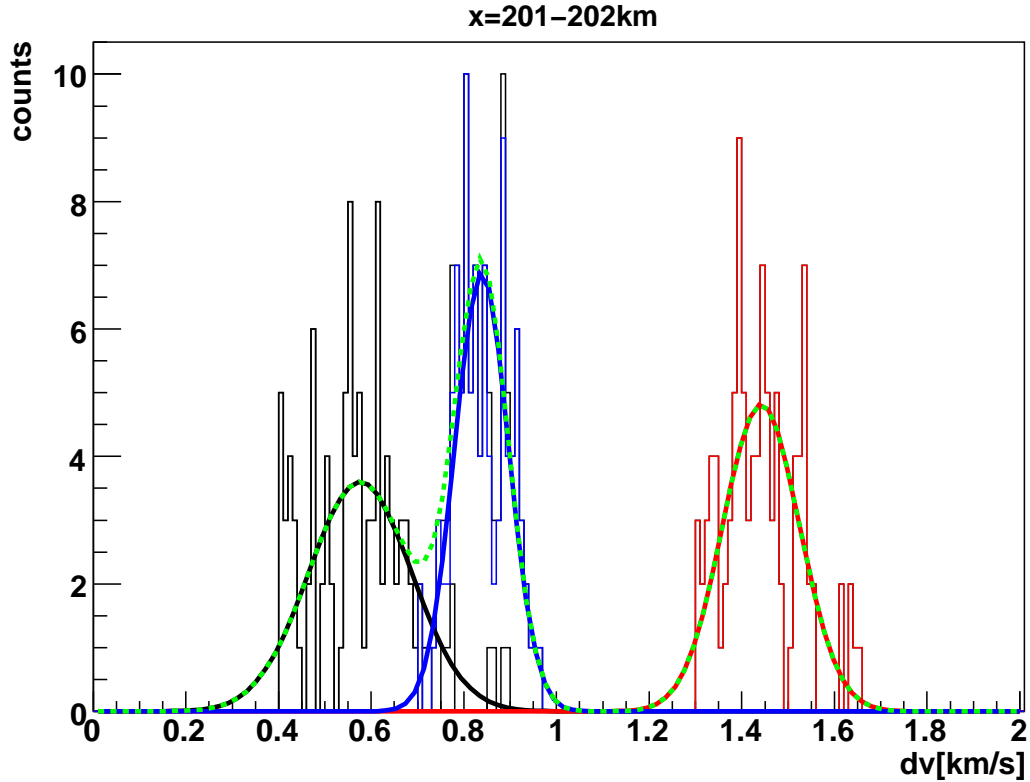


Figure 2.7: Example of the overlap of the cumulative divergence Δv in the transition zone from the forearc high into the accretionary complex. The distributions are projected in the Δv plane and subsequently fitted with Gaussian functions. The green curve corresponds to equation 2.7.

identifiable due to the mixing of the island arc and accretionary complex distributions Δv_1 and Δv_3 (Figure 2.6). Between km 165 and 190 we see how the distributions interchange their divergent behaviour.

Besides the small scale structures which are mimicked by the match to the mean curves we can clearly define regions of accretionary, forearc, and island arc character (Figure 2.6). Moving along the profile we enter the forearc high at km 130 and leave it at km 180 where we enter a sedimentary basin from km 180 to 190. Strong mixing and a sudden increase in the uncertainty of the fit result indicate a structural change

between an island arc and a velocity field characteristic of a sediment accretionary prism. At km 202 the divergence seems to be large to each fit (Figure 2.7). One reason for this might be a velocity increase related to a geologic-tectonic backstop feature identified here in previous studies (Bangs et al. (2003), Christeson et al. (2003)). The parametrization of the model space allows a direct comparison between the velocity structure of a tomographic solution and an assumed velocity distribution for a defined tectonic setting. Furthermore we can test different tectonic settings given a mean velocity distribution for each one of them. The statistics obtained by variable starting models in a monte carlo ensemble helps defining tolerance intervals for the deviation. We chose two schemes of comparing the velocity structure along the profile. The first method allows an overall estimation of conformity (χ^2/rms) between the velocity structure at a given x position up to a certain depth in a tomographic solution and the velocity structure we would expect for a predefined tectonic setting. This provides an overall estimate of the divergence along the profile for a tectonic setting (x -estimation). A different approach is a singular comparison of velocity values resulting in a deviation between expected (reference) and calculated (model) values. This yields an estimate of structural change moving deeper in the model, and allows a comparison at particular depths (xz -estimation):

$$\Delta v_{1k_{max}}(x) = \sqrt{\frac{\sum_{k=0}^{k_{max}} (\bar{v}_1(x, z_k) - v(x, z_k))^2}{k_{max} - 1}}, \quad 1 \leq k_{max} \leq nz \quad (2.8)$$

$$dv_{1k}(x, z_k) = \sqrt{(\bar{v}_1(x, z_k) - v(x, z_k))^2} \quad (2.9)$$

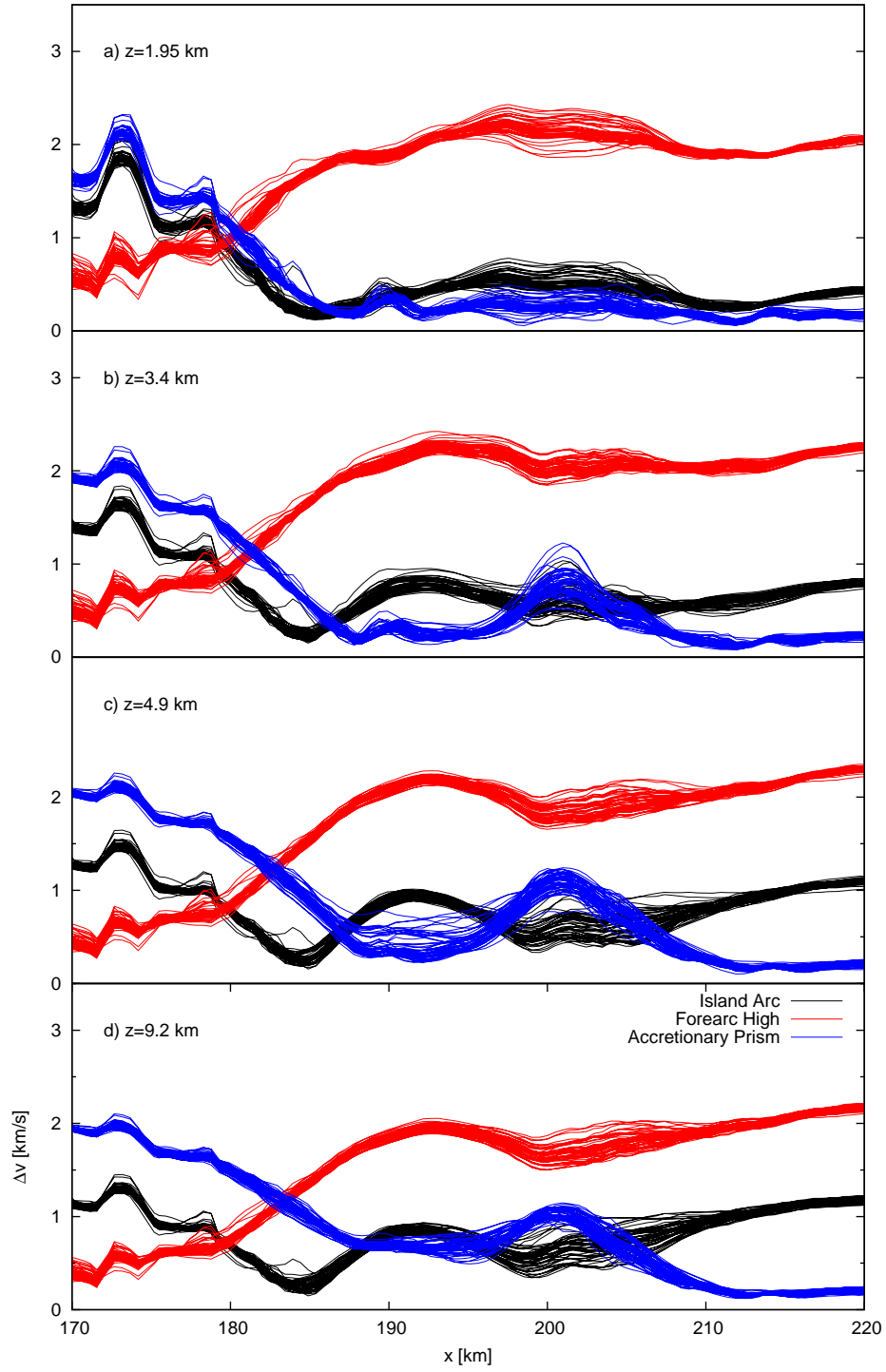
With these two methods it is possible to analyze the structural changes along the profile. We chose the three tectonic regions we used for the setup of the monte carlo ensemble for comparison to achieve a higher estimate of equivalence and divergence.

2.4 Analyzing the Backstop

The divergence in the transition zone between the forearc and accretionary region can be better understood by comparing Δv of equation 2.6 not over the complete range of

z ($k = 1 \dots n_z$) but sequentially moving deeper into the model ($k = 1 \dots k_{max}$; Equation 2.8). We would expect a higher resemblance to the accretionary distribution for the shallower terms, i.e. summation up to $k_{max} \ll n_z$, whereas the resemblance to the island arc velocity distribution would become predominant in the deeper part due to an increase in velocities. This is visualized in Figure 2.8 with increasing depth range. Figure 2.9 shows the distributions at a depth of 4.9 km below seafloor. If we analyze the mean distributions adding more and more values as we move deeper we see the structural change associated with the three tectonic regimes. This gives a qualitative measure of the velocity structure at a certain x position along the profile and consequently gives a regional approximation of the velocity field. The second approach we chose attempts a direct comparison of velocities at all z node positions along the profile (Equation 2.9; Figure 2.10). This is a 1 bin thick z -filter returning the deviation between the model and expectation values of the mean distributions. We move parallel to the seafloor and calculate the deviation at each position (x, z). This approach allows a direct match between the reference and calculated velocities. Since we compare with three different distributions we have an estimate of the structural setting. Furthermore we can provide tolerance intervals of the match to a given distribution by a Gaussian fit at each x position. At 195 profile km $z=2.9$ km below seafloor the mean velocity of the accretionary distribution at this depth is deviating, whereas the mean velocities from the fore- and island arc are matching. Further tracing the match at depth the behaviour can be mapped (Mosegaard and Tarantola (1995)). This is valid at each x node only where the raycoverage in the model is sufficient. Figure 2.10 shows the distributions at increasing depths below the seafloor. This yields a qualitative measure of the velocity

Figure 2.8 (following page): Cumulative divergence of actual $v(x_i, z_k)$ to the mean velocity up to depths of $z_k = 1.95km, 3.4km, 4.9km$, and $9.2km$ below the seafloor between profile $170 \leq x_i \leq 220$.



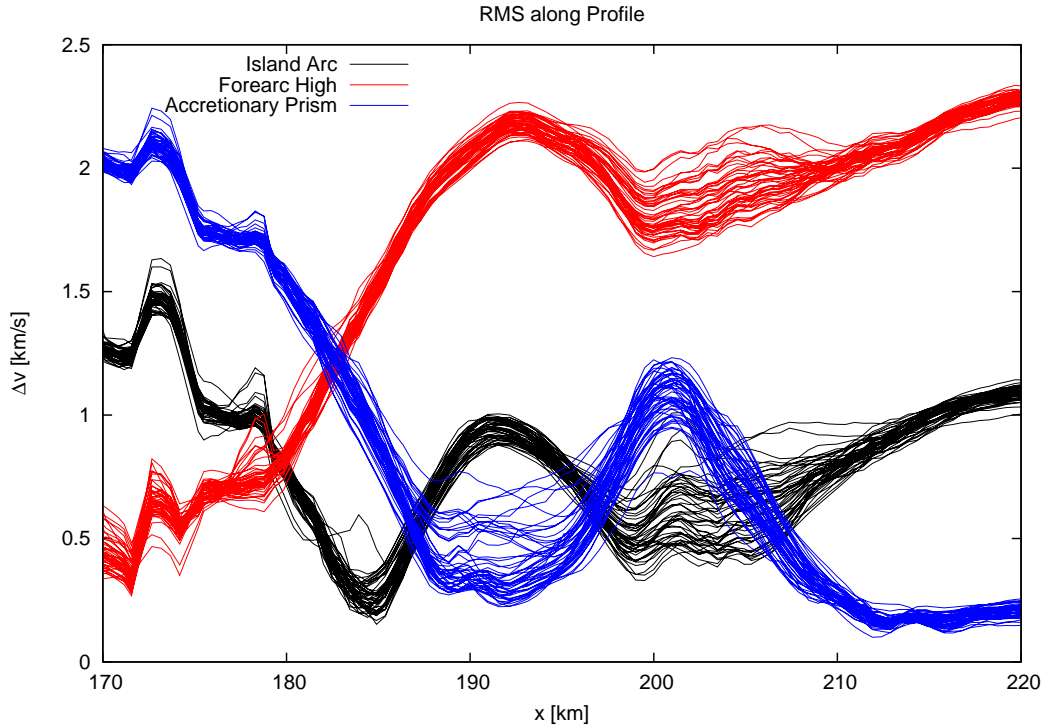


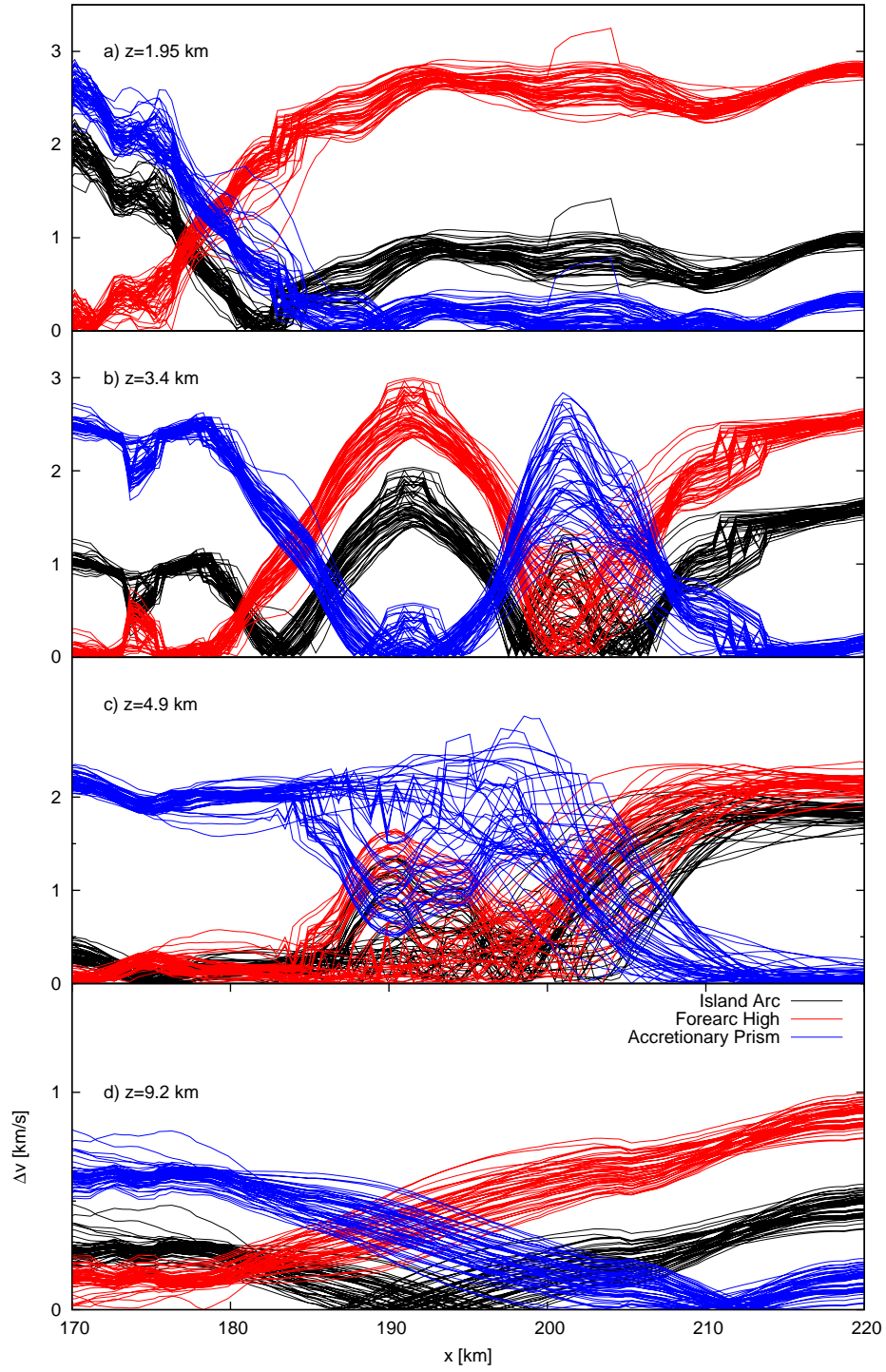
Figure 2.9: Distribution of Δv functions after fit for $z=4.9$ km ($k_{max} = 70$) below seafloor, showing a clear distinction in the velocity structure in the vicinity of the backstop feature.

structure at a certain x position and certain depth z . Comparing this with the previous method we see higher horizontal as well as vertical structural changes in the velocity field and obtain a quantitative measure of divergence for each (x,z) -node.

The maximum depths reached by the rays in this part of the profile range from 6.5-14.5 km below seafloor, which make a comparison in deeper parts of the profile impossible. This can also be seen in the lower panel of Figure 2.10 where no clear match is tracable.

The backstop (Bangs et al. (2003) and Christeson et al. (2003)) has been interpreted

Figure 2.10 (following page): Singular deviation of $v(x_i, z_k)$ for $170 \leq x_i \leq 220$ to the mean velocity at depths $z_k = 1.95\text{km}, 3.4\text{km}, 4.9\text{km},$ and 9.2km below the seafloor. Clear structural changes are visible below the seafloor.



by a match between tomographic and near-vertical data analysis. The comparison concluded in a best match of iso contours between 3.5km/s and 5.5km/s. Assuming a geological relationship between forearc and backstop we should be able to trace the velocity gradients according to this interpretation. Following is a 2-d filter design on the basis of the preceding interpretation gained by a divergence analysis. We choose to analyze the 2-d profile with the mean velocity distribution \bar{v}_2 between $v_{min} = 3.797$ and $v_{max} = 5.064$ ($15 \leq k_{div} \leq 25$). Figure 2.11 shows the divergence of the match moving deeper along the profile for a single model.

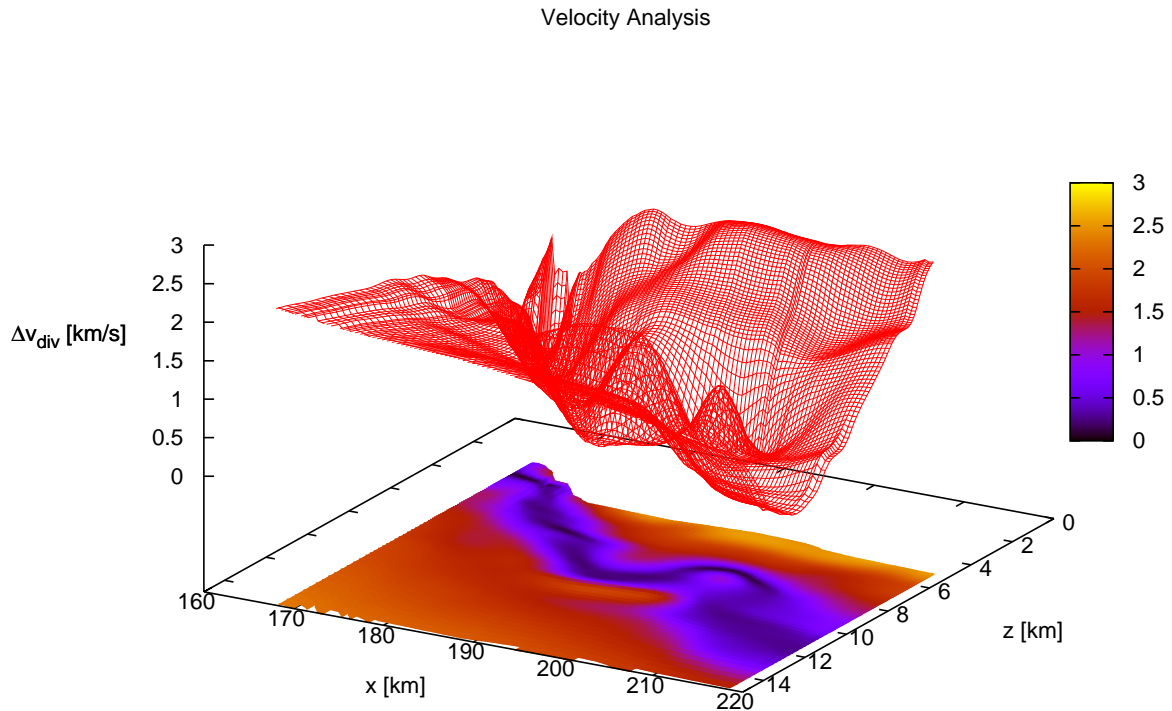


Figure 2.11: Example of the divergence for one output model moving deeper. The dark areas represent higher matching of the velocity structure in comparison to the mean curve \bar{v}_2

For each x-node we calculate the divergence dv at each z-node. Doing this for all Models we are able to retrieve a minimal matching distribution of the backstop structure.

Figure 2.12 shows a perspective view of this distribution and visualizes the fitting routine on finding the most probable, i.e. mean, values of the depths according to a best match between forearc and backstop. Projections of the distribution are made in depth and subsequently fitted with Gaussian functions. Figure 2.13 shows the result of minimal matching of all the models. The binning of the model is clearly visible and since we don't reach the same depths in forward calculating the rays in all of the models we could neglect certain results. This analysis is strongly dependant on the information to be gained by it, but in general applies to any facies in a purely homogeneous study you want to construct and if the search algorithm resembles what you are looking for.

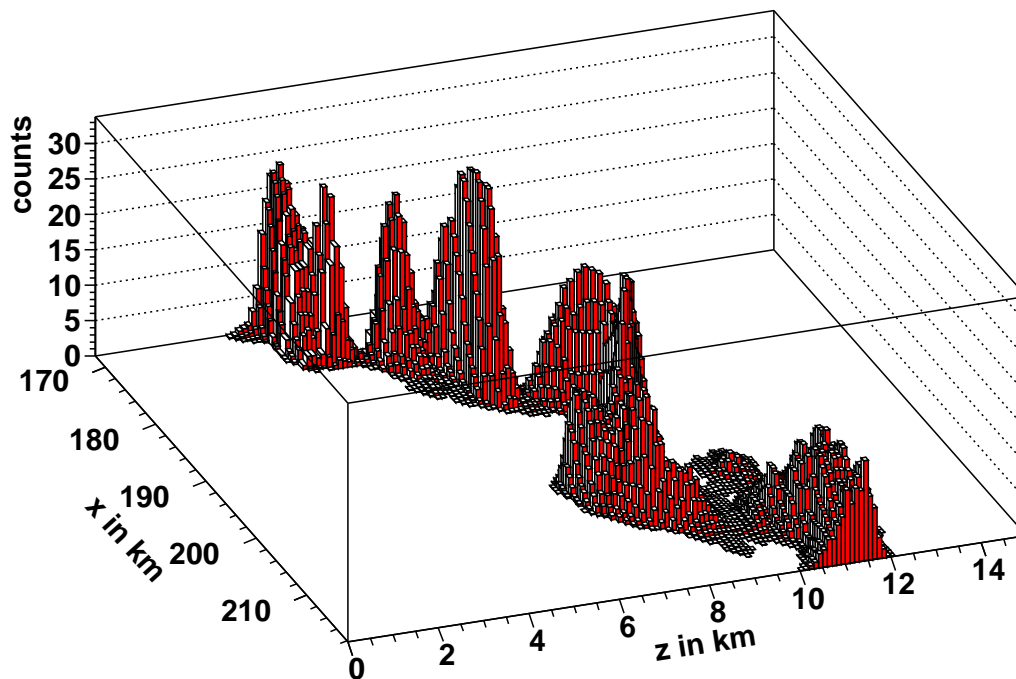


Figure 2.12: Perspective view of the backstop structure according to a divergence analysis with $15 \leq k_{div} \leq 25$. Projecting onto z-axis with subsequently fitting the result gives the most probable depths for the backstop along the profile.

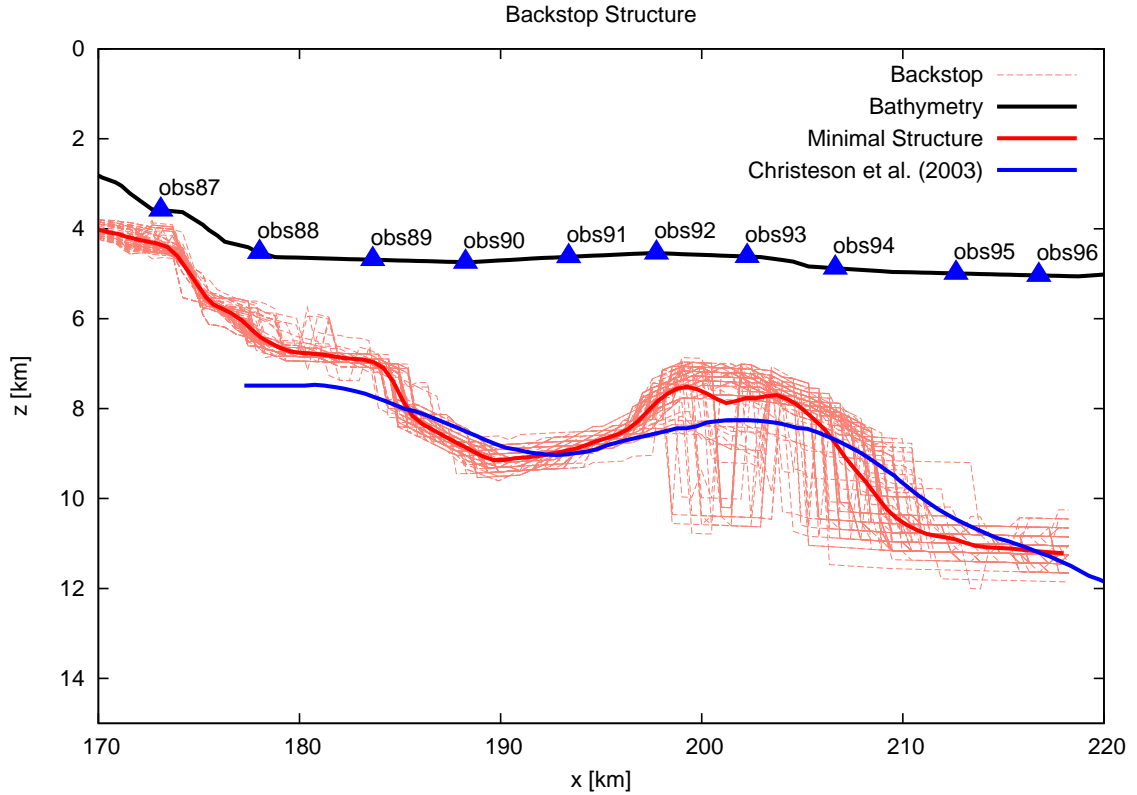


Figure 2.13: Backstop structure according to a divergence analysis with $\overline{v_2}(i, k_{div})$ $15 \leq k_{div} \leq 25$. The parametrization is clearly visible and the resolution decreases due to weaker penetration depths in the accretionary domain. The thick red curve denotes the minimal structure of the backstop and the blue line denotes the interpretation according to the 4.5 km/s iso contour line of Christeson et al. (2003)

2.5 Conclusion

From this study we infer several conclusions concerning the interpretation of the tomographic approach. By calculating a global as well as singular misfit of velocities we are able to map tectonic regions along the profile. Comparing velocity distributions with the result of a tomographic inversion along the profile we can mimic the subsurface structures in their extent and composition. The possibility of gaining a priori

information for seismic refraction analysis by a simple solution to an inverse problem and subsequent resolution of structural heterogeneities through a divergence analysis is a new and simple way of defining a priori space and estimating the a posteriori mean and covariance in singular and general form. The major advantage of a monte carlo based approach in our case study is the gained knowledge of velocity depth distributions. Certainly the decision of where to extract velocity information on the profile for setting up a monte carlo ensemble is limiting the a priori space. However, the general conclusion of analyzing the velocity field according to distinct reference distributions gives us the possibility to define the covariance according to any tectonic environment if we have a priori information on the velocity depth distributions. Using the wide-angle data recorded across the Lesser Antilles, we were able to resolve a shallow feature like the backstop by a robust and simple divergence analysis. We demonstrated the effectiveness of the new methodology to extract some key features and properties from the inversion results by including information concerning the confidence level of results. We present a new and simple approach of defining a priori space and estimating the a posteriori mean and covariance in singular and general form by a simple solution to an inverse problem and subsequent resolution analysis of structural heterogeneity by the proposed divergence analysis.

Chapter 3

Wide-Angle Modeling

Oceanic island arcs are sites of high magma production and contribute to the formation of continental crust. Geophysical studies may provide information on the configuration and composition of island arc crust, however, to date only few seismic profiles exist across active island arcs, limiting our knowledge on the deep structure and processes related to the production of arc crust. We acquired active-source wide-angle seismic data crossing the central Lesser Antilles island arc north of Dominica where the oceanic Tiburon Ridge subducts obliquely beneath the forearc. A combined analysis of wide-angle seismics and prestack depth migrated reflection data images the complex structure of the backstop and its segmentation into two individual ridges, suggesting an intricate relation between subducted basement relief and forearc deformation. Tomographic imaging reveals three distinct layers composing the island arc crust. A three kilometer thick upper crust of volcanogenic sedimentary rocks and volcanoclastics is underlain by intermediate to felsic middle crust and plutonic lower crust. The island arc crust may comprise inherited elements of oceanic plateau material contributing to the observed crustal thickness. A high density ultramafic cumulates layer is not detected, which is an important observation for models of continental crust formation. The upper plate Moho is found at a depth of 24 kilometers below the sea floor. Upper mantle velocities are close to the global average. Our study provides important information on the composition of the island arc crust and its deep structure, ranging from intermediate to felsic and mafic conditions.

3.1 Introduction

The role of magma production along intra-oceanic arcs in the formation of continental crust in the Phanerozoic has long been recognized (e.g. Clift and Vannucchi, 2004; Davidson and Arculus, 2008; Kodaira et al., 2007b,a; Tatsumi et al., 2008, and references therein), but an improved understanding of the associated tectono-magmatic processes requires an evaluation of the deep structure of these systems (e.g. Acocella and Funicello, 2010). The Lesser Antilles island arc is characterized by a low magma production rate related to the low rate of convergence (Macdonald et al., 2000). Segmentation of the margin is reflected in the variation of volcanic activity and geometry of the Benioff zone (Wadge and Shepherd, 1984; Huang et al., 2010) along the arc. The central Lesser Antilles arc around 16° N has been the site of a number of previous experiments (Westbrook et al., 1988; Bangs et al., 1990, 2003; Bangs and Westbrook, 1991; Christeson et al., 2003), which have mainly focused on the accretionary complex and backstop geometry. However, no seismic profile has been acquired traversing the central island arc itself, leaving the arc geometry and basement as well as Moho depth here undetermined. We present the results of a 280 km long regional wide-angle seismic profile conducted south of Guadeloupe between 15.5° N and 16.5° N, trending approximately perpendicular to the deformation front/parallel to convergence (Fig. 3.1). The profile initiates in the Grenada Basin, crosses the active island arc and extends onto the Barbados Ridge accretionary complex, where it terminates approximately 80 km west of the deformation front. A total of 44 ocean bottom seismic stations were deployed along the profile, which in addition was covered by multichannel seismic data along its northeastern extent (Fig. 3.1). The joint analysis of seismic refraction, wide-angle reflection and multichannel seismic data reveals a detailed image of the central Lesser Antilles margin. The study provides constraints on the previously unresolved deep crustal structure and upper mantle of the active Lesser Antilles island arc.

3.2 Regional Tectonic Setting And Previous Investigations

The Lesser Antilles are an active island arc formed by the subduction of old Atlantic crust (Lower Campanian-Maestrichtian) under the Caribbean plate. The strongly curved, ~ 850 km long Lesser Antilles subduction zone constitutes the eastern margin of the Caribbean plate (Westbrook, 1975) and absorbs the ENE motion between the North American and the Caribbean plates that converge at a rate of 2.1 cm/a (DeMets et al., 2000) (Fig. 3.1). Crustal thickness of the Caribbean plate is intermediate between typical continental and oceanic values. This is compatible with thickened oceanic crust of Pacific origin modified and thickened during passage over the Galapagos hotspot prior to emplacement between the Americas (Mauffret, 1997). The Caribbean igneous province is characterized by a number of volcanic plateaus and closely resembles large igneous provinces such as Kerguelen or Ontong-Java. Deep basins of thinner crust with underplated volcanic material separate the plateaus (Mauffret, 1997). Additional crustal thickening may be associated with Eocene-Oligocene magmatic activity of the Antilles volcanic arc. To the west of the Lesser Antilles Arc lies the Grenada Basin, which is bordered on its western side by a remnant arc, the Aves Ridge (Fig. 3.1 inset) (Boynton et al., 1979). The origin of the Grenada Basin remains enigmatic. The velocity structure determined in the southern Grenada Basin around 12° N is consistent with oceanic crust formed by backarc spreading or alternatively sourced from the forearc region (Christeson et al., 2008, and references therein). Near our study area north of 15° N, water depth in the marine backarc domain is significantly less than that of the incoming Atlantic oceanic lithosphere. Shallow water may be considered as indicative of a lower density lithosphere. In the oceanic domain, this is commonly regarded to be easiest achieved by thickened crust, e.g. by magmatic underplating. The complex history of the Caribbean region and the presence of a number of oceanic plateaus imply that the original primitive crust has been altered by intrusion and extrusion of volcanic material and possible thickening by deep magmatic processes, which have modified the crustal velocity structure (Mauffret, 1997).

Our experiment was conducted along the central Lesser Antilles margin between the islands of Dominica and Guadeloupe (Fig. 3.1). Here, the active island arc is situated approximately 280 km west of the deformation front. The complex, episodic magmatic history of the margin resulted in two main volcanic fronts (Bouysse, 1988) from Martinique (Fig. 3.1 inset) northwards, where the recent arc, which is active since the early Miocene, is progressively offset to the west. As a result, the island of Guadeloupe is partitioned into two parts of different volcanic origin in the east (Grande Terre) and west (Basse Terre) (Fig. 3.1). The separation of the recent, active arc and the older Eocene to mid-Oligocene arc is proposed to be the result of kinematic changes in the subduction processes in the late Oligocene (Bouysse, 1990). Pleistocene to recent (<2 Ma) magmatic activity is focused in a narrow band (<10 km wide) along the western volcanic front (Macdonald et al., 2000). Early gravity modeling combined with limited seismic information estimated a crustal thickness of 30-35 km for the central and northern Lesser Antilles Arc (Westbrook, 1975; Boynton et al., 1979; Maury et al., 1990). A receiver function study imaged a crust thickness of ~ 30 km on average for the Montserrat region (Fig. 3.1) with values ranging from 26 km to 34 km (Sevilla et al., 2010) and thus slightly thinner than the earlier estimates. Near the southern termination of the Lesser Antilles island arc, a crustal thickness of ~ 24 km was determined from refraction seismic data (Profile TRIN in Fig. 3.1; Christeson et al., 2008).

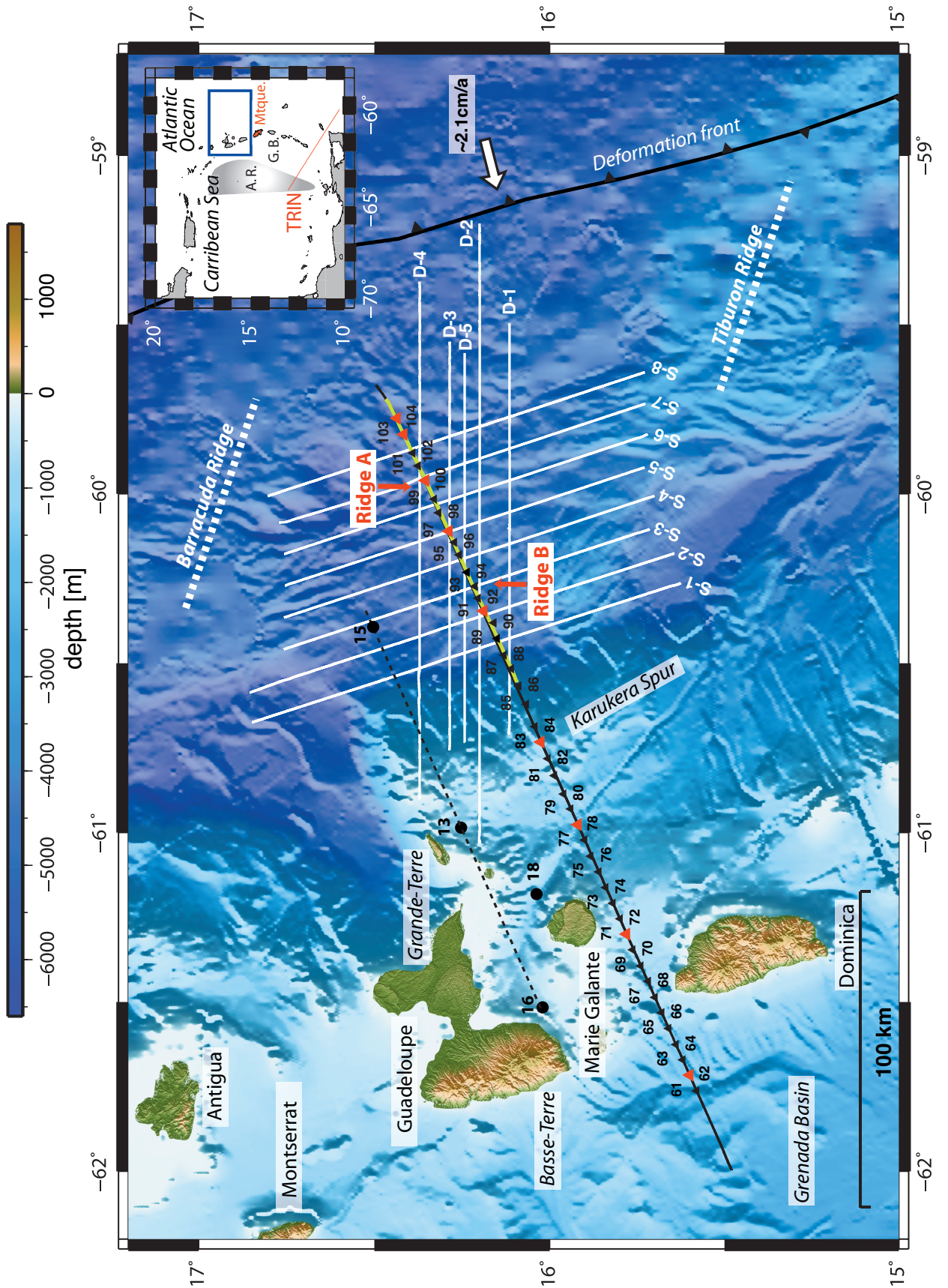
The Lesser Antilles forearc is dominated by a significant accretionary prism termed the Barbados Ridge accretionary complex, which forms by subduction accretion initiated in the Eocene. In our study area, approximately 1/3 of the sediment input along the portion of the margin coinciding with our study area is frontally accreted, while the remaining ~ 500 -700 m of sediment are underthrust beneath the accretionary prism adjacent to the deformation front (Westbrook et al., 1988). The prism has a width of ~ 125 km here, decreasing northwards. To the south, the accretionary wedge reaches a width of more than 300 km and 20 km in thickness where it approaches the sediment source associated with the South American river systems (Westbrook, 1975; Westbrook et al., 1982).

An abrupt westward retreat (~ 100 km) of the deformation front occurs east of the

island of Martinique and is related to the oblique subduction of the Tiburon Ridge, which blocks sediment transport to the north (Fig. 3.1). The portion of the Tiburon Ridge expressed in the topography of the Atlantic seafloor is 150 km long and 30-40 km wide and rises 1850 m above the surrounding oceanic basin, trending in a WNW direction (Bangs et al., 2003). To the north, east of the deformation front offshore Guadeloupe, a second aseismic ridge, the Barracuda Ridge, extends for more than 390 km onto the abyssal plain in a WNW direction, parallel to the Tiburon Ridge (Fig. 3.1). The Barracuda Ridge displays an irregular width, ranging from less than 25 km to ~ 60 km along its eastern termination. Both ridges profoundly modulate the margin architecture and geometry, causing local uplift of the forearc.

Our seismic line crosses the location of the coincident seismic reflection/refraction grid of Bangs et al. (1990; 2003) and Christeson et al. (2003) (Fig. 3.1) along the forearc basin and outer forearc high, which revealed the igneous forearc crust, forearc basin and accretionary wedge structure near 16° N. In particular, the island arc crust that serves as backstop to the accretionary prism was imaged in great detail. The deeply buried island arc crust is characterized by considerable relief as documented by two ridges (Ridge A and Ridge B) rising 1-6 km above the adjacent basement (Christeson et al., 2003) and possibly incorporates fragments of an accreted aseismic ridge at its toe (Bangs et al., 2003). The forearc basin sediments above the backstop are only mildly deformed in contrast to the accretionary prism fronting the island arc crust. The accretionary wedge shows little lateral variation across its 125 km width and only minimal backthrusting over the island arc crust (Bangs et al., 2003).

Figure 3.1 (following page): Location map of wide-angle seismic profile with ocean bottom stations indicated by triangles. The northeastern portion of the profile marked in yellow was additionally covered by multichannel reflection data. The Tiburon and Barracuda ridges subduct obliquely underneath the forearc. White lines (D1-D5; S1-S8) indicate seismic grid by Bangs et al. (2003) and Christeson et al. (2003). Dotted line indicates location of refraction profile with four ocean bottom stations (black dots) discussed by Roux (2007). Inset shows regional tectonic framework and location of the TRIN profile across the southern Antilles (Christeson et al., 2008). Study area indicated by black square in the inset. A.R.: Aves Ridge, G. B.: Grenada Basin, Mtque: Martinique.



In a reconnaissance experiment (SISMANTILLES I) multichannel seismic reflection data (MCS) were acquired offshore Guadeloupe and Martinique in 2001 (Laigle et al., 2005; Roux, 2007) and shots were recorded by a limited number of ocean bottom seismometer (OBS) receivers as wide-angle refraction profiles (Fig. 3.1). For logistical reasons shotlines could not penetrate to less than 1000 m water depth, that is onto and west of the Karukera Spur (~ 80 km east of the volcanic arc) (Fig. 3.1). East of it only shooting was extended and with a halfpower source, and only the easternmost OBS was in a position to record at a long range, but as an unreversed profile. Hence sampling of deep structure was restricted to under the accretionary wedge and the outer forearc. There, the deepest refractor evidenced at 10-15 km depth with a velocity >7 km/s appeared consistent with the interpretation as forearc Moho (Roux, 2007) as found at such depths in the case of intra-oceanic or Island arc type subduction zones, such as Alaska-Aleutian (e.g. Holbrook et al., 1999; Lizarralde et al., 2002), Mariana (e.g. Takahashi et al., 2007), Izu Bonin Mariana (e.g. Suyehiro et al., 1996), and Java (Kopp et al., 2002).

3.3 Data Acquisition and Processing

In January-February 2007 the 'Thales was Right' project investigated the central Lesser Antilles arc system between 14.5° N and 17.5° N with the German R/V Maria S. Merian (TRAIL cruise MSM04/2) and the French N/O L'Atalante (SISMANTILLES II cruise). During the TRAIL cruise, a refraction seismic line was acquired north of the Republic of Dominica, extending in a SW to NE direction and partially coincides with a reflection profile acquired during the SISMANTILLES II and SUBSISMANTI cruises of N/O L'Atalante of IFREMER (Fig. 3.1). The seismic refraction profile was shot with a 5-element seismic source array with a trigger interval of 60 s at a ship speed of 3.7 kn on average, resulting in a shot spacing of approximately 100 m. Standard processing of the OBS data included clock drift correction and relocalization using the water wave arrival and exact shot geometry. Subsequently, a time-gated deconvolution removed predictable bubble reverberations to produce a clean signal without disturbing interference of multiple and primary phases. In a

second step, a time and offset-variant Butterworth filter was designed to account for frequency changes caused by signal attenuation. The filter's passband continuously shifts towards lower frequencies as offset and record time increase. Clear first arrivals are observed to an average offset of 60-70 km on the Caribbean Plate. Signal-to-noise ratios vary considerably and clear arrivals on some stations could be traced to 100-130 km offsets.

Following the OBS experiment, MCS data coincident on the deeper eastern part of the transect were recorded with the N/O L'Atalante using a 4.5 km long, 360 channel digital streamer and a 8865 cu.in Bolt air gun. The reflection data were gathered to reveal the sedimentary structures as well as fault deformation patterns to gain a priori information on the upper layers as input to the refraction seismic modeling. MCS processing included prestack processing and pre-stack depth migration. A time-space-variant frequency filter was applied prior to a predictive deconvolution (prediction window from 80 ms to 480 ms) and spherical divergence correction. Normal moveout correction and velocity analysis was followed by multiple suppression conducted in the tau-p-domain and common depth point stacking. For the pre-stack depth migration, we chose an iterative scheme using focusing analyses and common reflection point gathers (Mackay and Abma, 1993) to determine seismic interval velocities. The wide-angle velocity model served as input to the first macro-model for the pre-stack depth migration and was subsequently updated during several iterations.

3.4 Tomographic Inversion

A two-dimensional velocity-depth model (Fig. 3.2a) was obtained using the joint refraction and reflection tomographic inversion method of Korenaga et al. (2000). This tomography scheme allows a combined inversion of refracted as well as reflected phases. It employs a hybrid raytracing scheme combining the graph method with further refinements utilizing ray bending with the conjugate gradients method. The velocity field v_{ik} is parameterized by a homogeneous grid of nodes (x_i, z_k) with $1 \leq i \leq n_x$ and $1 \leq k \leq n_z$ hanging below the seafloor. We chose a lateral nodal spacing of 0.5 km and an increasing vertical nodal spacing ranging from 0.05-1.0 km. To

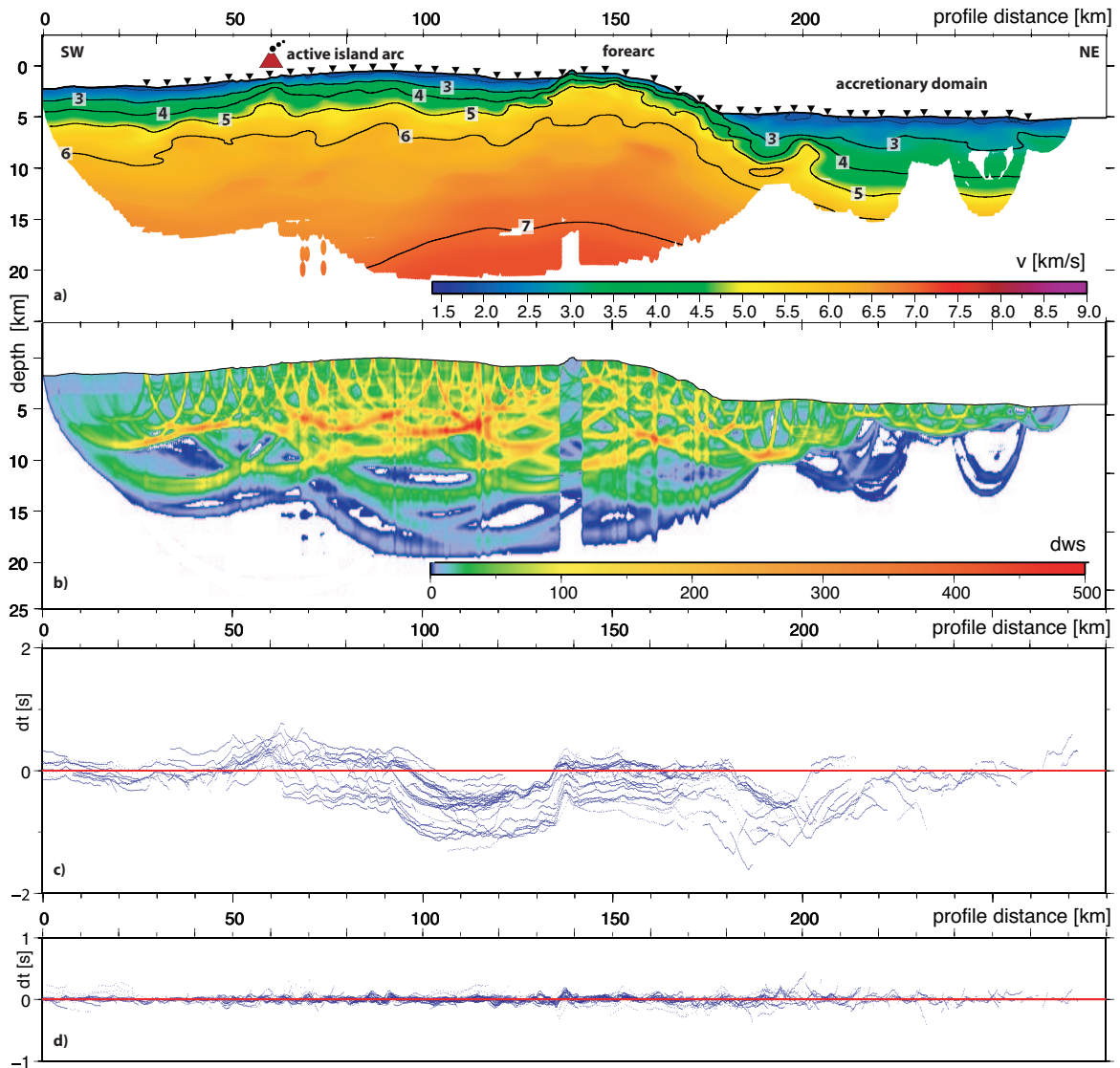


Figure 3.2: (a) Joint refraction and reflection tomographic inversion across the Central Lesser Antilles island arc. Numerals indicate v_p velocities in km/s. Triangles indicate ocean bottom seismic stations and red volcano shows location of the active volcanic front. Only resolved areas are displayed. Three distinct tectonic regions are resolved: the accretionary domain, the forearc and the active island arc. (b) Derivative weight sum (DWS) of rays traveling through the model provides an estimate for the potential model resolution. (c) Initial and (d) final root-mean-square (RMS) misfits. The resulting residuals are in the order of 50 ms.

account for a geometrical effect evolving from a local basement high structure we re-sampled the lateral spacing in a 8 km wide region from 136-142 profile km (Fig. 3.2b). Depth dependant smoothing constraints and correlation lengths ranging from 1-5 km horizontally and 0.1-1 km vertically were used to stabilize the inversion. A simple layered 1-D velocity model served as the starting model for the initial tomographic inversion. The result of this inversion provided an estimate of the velocity structure along the transect and supplied the basis for defining three distinct tectonic units of the margin, namely the active island arc (1), forearc domain (2) and accretionary domain (3) (Weinzierl and Kopp, 2010) (Fig. 3.2a). The velocity distribution and

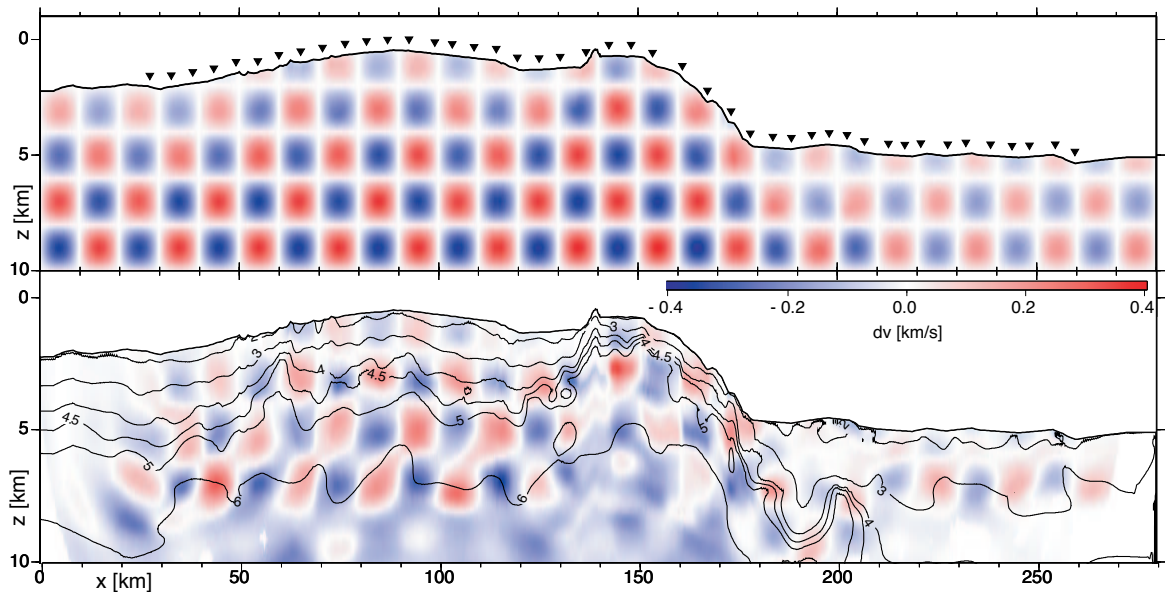


Figure 3.3: Checkerboard test to analyse the spatial and amplitude resolution along the profile. A checkerboard pattern of 2x10 km (vertical x horizontal) is adequately resolved to a depth of 10 km. Amplitude variation is $\pm 6\%$.

segment definition are in accordance with earlier seismic refraction tomography results (Christeson et al., 2003). We chose a conservative picking strategy and manually picked the first arrival travel times only where arrivals could be picked within an error range of 30-100 ms, resulting in a total of more than 22500 picks (Fig. 3.2c); no

picks were placed where the signal-to-noise ratio inhibited exact picking. RMS travel time misfits for the final velocity model are in the order of 50 ms (Fig. 3.2d). The spatial and amplitude resolution of the tomographic inversion, which depends on the ray geometry and seismic velocity field, was analysed using a checkerboard test. The final inversion is perturbed by a checkerboard pattern of 2 x 10 km (vertical x horizontal checker size) using values of $\pm 6\%$ between the seafloor and 10 km depth (Fig. 3.3). Subsequently, synthetic traveltimes are computed through the perturbed medium, using the same sourcereceiver geometry as for the tomographic inversion. The tomography is then re-calculated based on the synthetic traveltimes in order to recover the initial perturbation pattern. Adequate resolution is achieved to a depth of approximately 8 km, which corresponds to basement depth underneath the active island arc (Fig. 3.3). As the resolution depends on the ray coverage, recovery breaks down along the profile's periphery.

3.4.1 Combining the near-vertical and wide-angle data

After performing the first-arrival tomography we used the retrieved velocity field as input for a pre-stack depth migration of the MCS data. Figure 3.4 displays the tomography velocity distribution used in the input macro-model of the pre-stack depth migration (Fig. 3.4a) and the velocity field of the last migration iteration (Fig. 3.4b), respectively. The joint analysis of the wide-angle and reflection seismic data is based on coincident acquisition geometries. The two resulting velocity models retrieve similar velocity trends, however, due to slightly diverging acquisition geometries, some details differ. The linedrawing is based on the pre-stack depth imaging (Fig. 3.4c-d). The decollement zone (Fig. 3.4d) is traced in the MCS image to a depth of 16 km, where it becomes difficult to distinguish from the framework rock (Fig. 3.4c). The decollement and the top of the oceanic basement (yellow and purple stippled lines in Fig. 3.4c) are also observed on stations deployed in the accretionary domain. A steeply seaward dipping fault is observed between km 235 -245 (turquoise line in Fig. 3.4c) and is identified on stations 100 and 103 (Fig. 3.5). Seismic reflectivity changes across this boundary, which marks the seaward extent of the forearc basin

and backstop and serves as a structural backbone to incoming sediments. The basement underneath the forearc basin (blue line in Fig. 3.4c) shows a highly variable topography and may be traced to the backstop fault and in the refraction data (Fig. 3.5).

Table 3.1: Phase nomenclature for wide-angle seismic data.

Phase	Description
Psed	Sedimentary phases
Pg	Refraction through the crust
PfbP	Reflection from the forearc basement
PbsP	Reflection from the backstop thrust zone
PdecP	Reflection from the decollement
PtocP	Reflection from the oceanic basement
PmPoc	Reflection from the crust-mantle boundary of the oceanic plate
PicP	Reflection from middle / lower crust interface
PmP	Reflection from the crust-mantle boundary of the Caribbean Plate
Pn	Refraction through the upper mantle

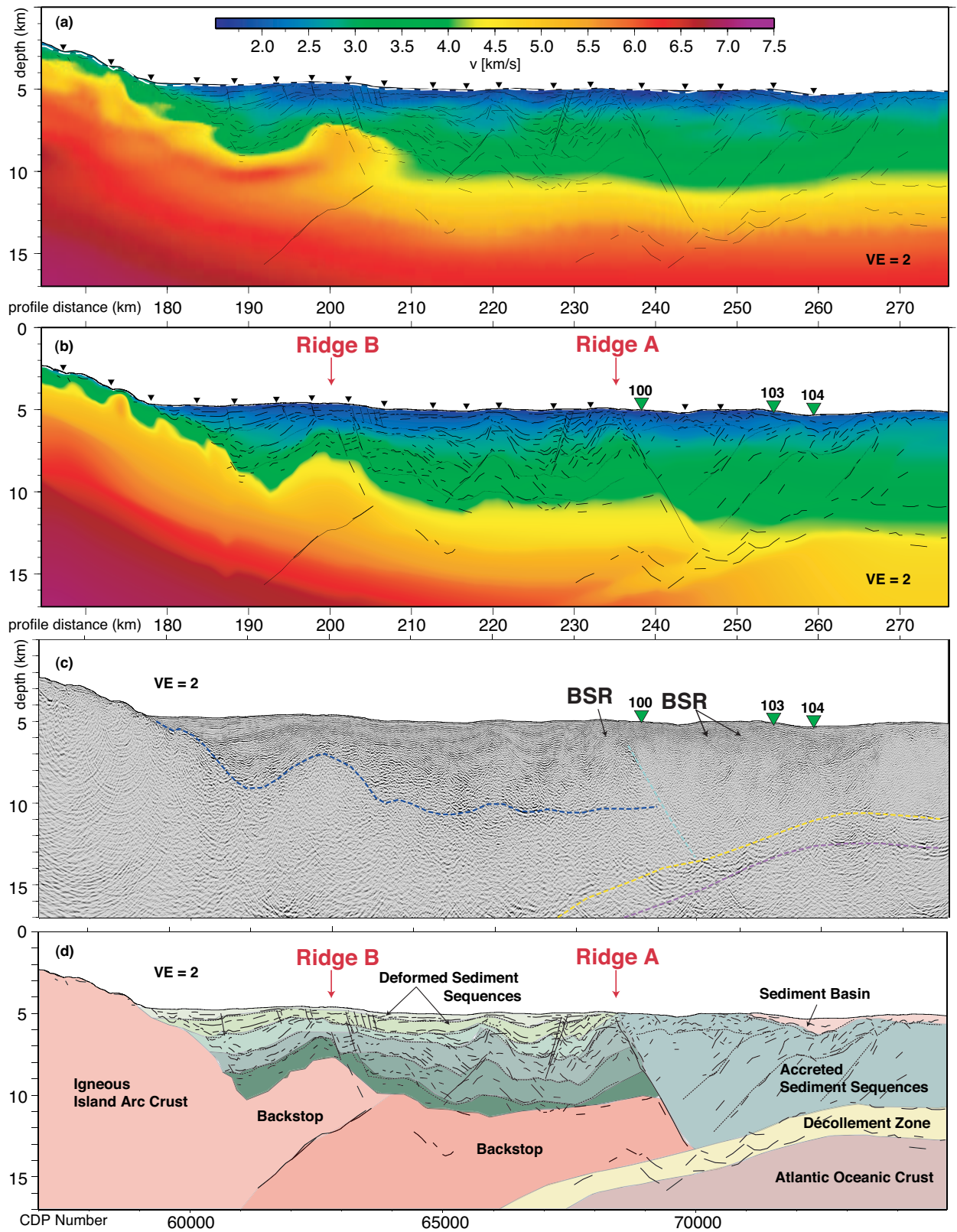
3.5 Forward Modeling

Owing to the complexity of the margin geometry and to account for secondary arrivals we used the tomography result to construct a forward model. This approach is advantageous because detailed a priori information on the velocity-depth distribution and the geologic structure along our profile's northeastern extent exists from previous studies (Bangs et al., 2003; Christeson et al., 2003) and may thus be incorporated into a layered forward model, which allows first order velocity discontinuities (Fig. 3.6). We used the hybrid forward/inverse travel time code provided by Zelt and Smith (1992), which employs a damped, least-squares approach to minimize travel time residuals. Inversion for interface depth with an upper structure determined by first arrival tomography can exploit the complementary nature of the subjective forward

and tomographic approach (Zelt et al., 2003). The final model of the first arrival travel time inversion (Fig. 3.2a) was used as a starting model converted into 6 layers by extracting iso-velocity contours along the transect where the travel time fit did not exceed our desired error estimate of 0.05 s. The upper portions of the model, which were well constrained by the tomography and pre-stack depth migration results, were kept fixed. In addition to the first arrivals already used in the tomographic inversion, we picked an additional 3611 secondary arrivals for the forward modeling.

The decollement and the top of the downthrusting oceanic crust underneath the accretionary wedge are traced by clear near-vertical reflections PdecP and PtocP (see 3.1 and e.g. OBS 103 in Fig. 3.5). Moving towards the island arc, the oceanic Moho is constrained by PmPoc reflections from underneath the backstop (OBS 97 in Fig. 3.7). Stations 97 and 91 document the lateral increase in seismic velocities from the forearc high to the island arc crust (backstop) (Pg phases in Fig. 3.7). A weak PmPoc phase (oceanic Moho reflection) is visible on station OBS 83 (Fig. 3.8) at 60-80 km

Figure 3.4 (following page): Combined analysis of wide-angle and reflection data. (a) final tomographic velocity model for the accretionary domain. This velocity distribution was used as input for the initial macro- model of the pre-stack depth migration of the multichannel reflection data. Linedrawing based on the reflection image presented in (c). Triangles indicate locations of ocean bottom stations. (b) final velocity model retrieved by depth focusing analysis during pre-stack depth migration of the multichannel data. Linedrawing is identical to (a). Ridge A and B are based on the interpretations by Bangs et al. (2003) and Christeson et al. (2003). (c) pre-stack depth migrated section across the accretionary domain and forearc basin. Discontinuous bottom simulating reflections (BSR) are indicative of gas hydrates. Stippled lines indicate the decollement (yellow), oceanic basement (purple), backstop thrust (turquoise) and forearc basement (blue) modeled by stations 100, 103-104 as presented in Figure 3.5. (d) interpretive section based on the velocity model presented in (b) and the pre-stack imaging shown in (c). The decollement zone dips gently underneath the thrust packages of the accretionary prism (240-275 km offset). A steeply seaward dipping fault marks a change in reflectivity and the transition to the forearc basin and backstop at depth. This fault forms the eastern flank of Ridge A. To the west, Ridge B deforms the overlying sediment layers trapped in the forearc basin. A landward dipping fault at 10-15 km depth around 190-200 km offset demonstrates that the two ridges form individual blocks as proposed by Bangs et al. (2003).



offset, tracing the Atlantic crust-mantle boundary to around 40 km depth. Secondary arrivals identified on stations located on the island arc crust reveal an intracrustal impedance contrast (PicP) in addition to the crust-mantle boundary (PmP) (Fig. 3.9). These arrivals are accounted for by incorporating an intracrustal boundary in the island arc crust during modeling (Weinzierl, 2010). Based on PmP reflections (e.g. OBS 71 in Fig. 3.8), the upper plate Moho is placed at 28 km depth with upper mantle velocities of 8.0 km/s.

3.6 Results

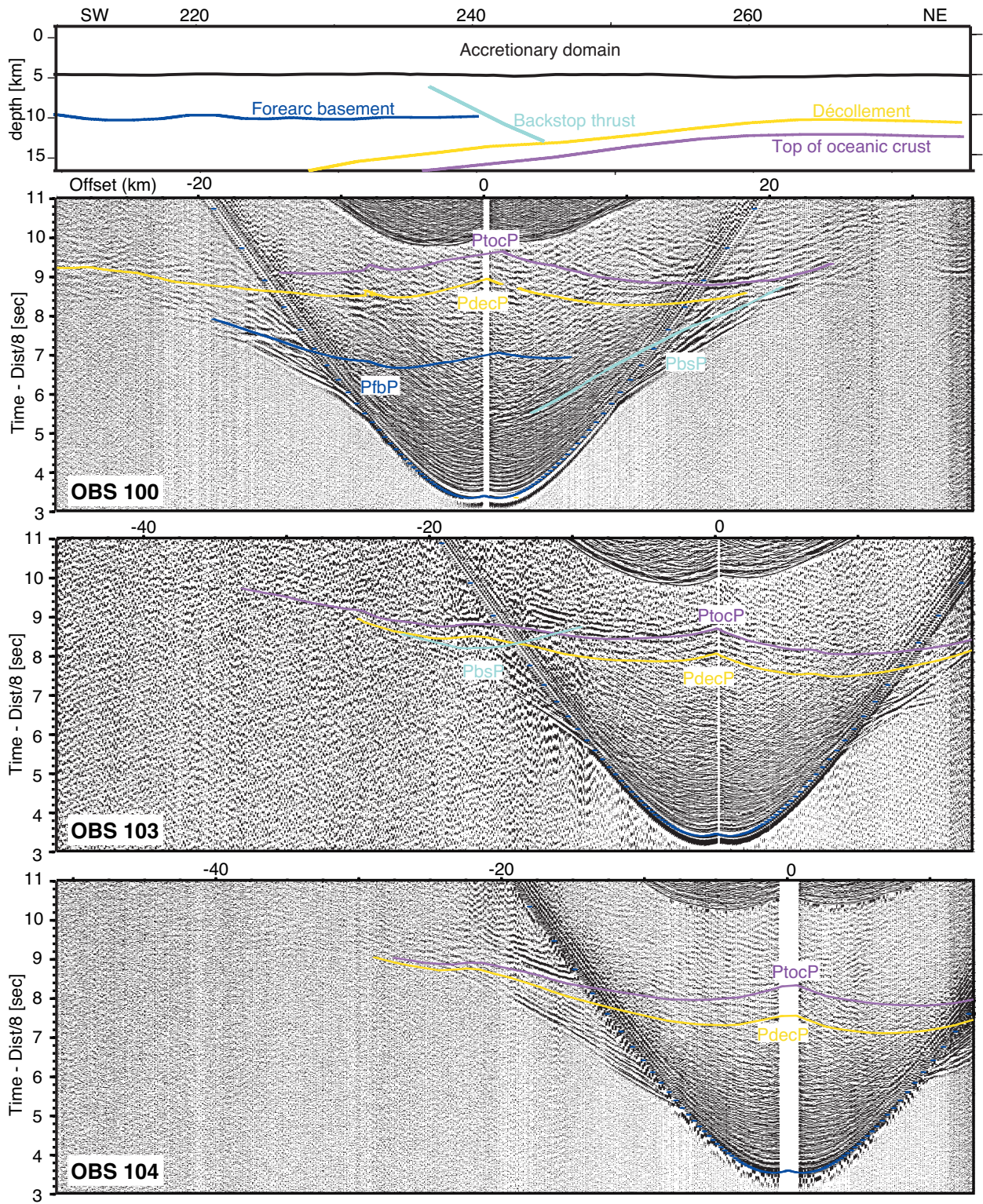
On the incoming plate, the wide-angle results reveal an 8 km thick oceanic crust below the accretionary prism and forearc high (Fig. 3.6). Underneath the island arc crust around profile km 200, the slab dips at an angle of $\sim 14.5^\circ$, steadily increasing underneath the island arc. Velocities of the incoming oceanic crust rise from 5.5 km/s at the oceanic basement to 7.3 km/s above the crust-mantle boundary. A distinction between oceanic layers 2 and 3 is not resolved (Fig. 3.6). Due to the lack of refracted mantle phases, upper mantle velocities of the subducting slab also remain unresolved. A decollement zone is imaged on the reflection profile (Fig. 3.4c) as well as on selected wide-angle record sections (e.g. OBS 103 in Fig. 3.5) and is characterized by low seismic velocities (~ 3.6 km/s) and a thickness of 1.3–1.8 km. Previous investigations of the lower slope and accretionary wedge approximately 70–80 km to the east of our profile imaged 0.5–0.75 km of sediment underthrust beneath the prism within the decollement zone (Westbrook et al., 1988; Bangs and Westbrook, 1991; Bangs et al., 1990, 2003). At the northeastern termination of our profile, the accretionary wedge is defined by seismic velocities ranging from 2.0 km/s near the surface to over 4.0 km/s at the decollement; the wedge gradually thickens to 40–45 km towards the island arc with little lateral variation in seismic velocities (Fig. 3.6). The approximate 30 km of MCS data covering the accretionary wedge between profile km 245–275 resolve the thickening of the wedge by imbricate thrusting (Fig. 3.4). Apart from the thrusts, few coherent reflections are imaged, other than strata trapped in a small basin (profile km 260). A discontinuous bottom-simulating reflector at a depth of 1 km bsf mimics

the seafloor (Fig. 3.4c) and indicates the presence of gas hydrates, as is common for many accretionary wedges worldwide (Waite et al., 2009), however, was previously not observed for the Lesser Antilles.

Previous seismic investigations on a grid of profiles imaged the backstop geometry and resolved two ridges (Ridge A and Ridge B, Fig. 3.1) (Bangs et al., 2003; Christeson et al., 2003). Ridge A is bounded by the seaward-dipping fault (turquoise stippled line in Fig. 3.4c) and marks the transition from the seaward forearc high to the forearc basin and is associated with laterally increasing velocities retrieved in the pre-stack depth migration (Fig. 3.4b). This velocity increase causes a moderate upward bending of velocity isolines in the tomographic inversion (Fig. 3.2) and forward model (Fig. 3.6) around profile km 230. Moving towards the island arc, Ridge B is resolved by our inversion results (profile km 190-210; Fig. 3.6) with seismic velocities exceeding 5.0 km/s, which corresponds to the results of Christeson et al. (2008). Ridge B is also imaged in the MCS data (Fig. 3.4) and correlates to a moderate uplift of the seafloor by several hundred meters. The variation in seafloor topography in this 2-D cross section, however, is of lower magnitude than the corresponding trend of the basement reflector. A steeply seaward vergent fault indicates a structural boundary below 10 km depth (profile km 240, Fig. 3.4c).

The steep slope in the seafloor topography ~ 20 km southwest of Ridge B marks the transition to the active island arc. Here, the seafloor rises by 3900 m and seismic velocities abruptly increase from the forearc basin sediments to the island arc crust (from 2.5 km/s to over 4.5 km/s) (Fig. 3.4c-d). As inferred from low seismic velocities of < 3.0 km/s, the island arc is covered by a sediment layer increasing in thickness from a few hundred meters near the forearc basin transition to 1100 m at the transition

Figure 3.5 (following page): Selected record sections of stations located on the accretionary prism (exact location shown in Figure 3.4c). These stations show clear arrivals from the structural interfaces displayed in the upper panel: the decollement (yellow), oceanic basement (purple), backstop thrust (turquoise) and forearc basement (blue). Modeling was conducted in the final velocity model used in the migration of the MCS data and displayed in Figure 3.4b. Boundaries shown in upper panel are identical to structures displayed in Figure 3.4c. Phase nomenclature given in Table 3.1.



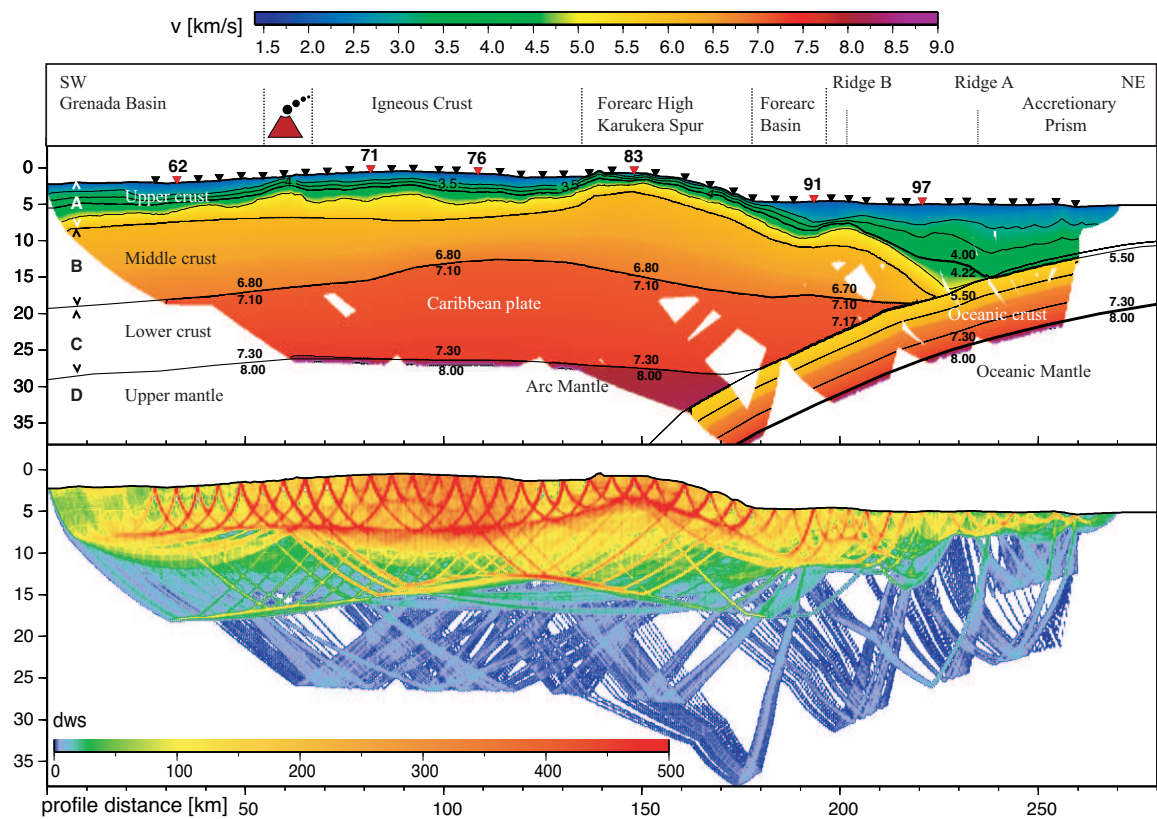


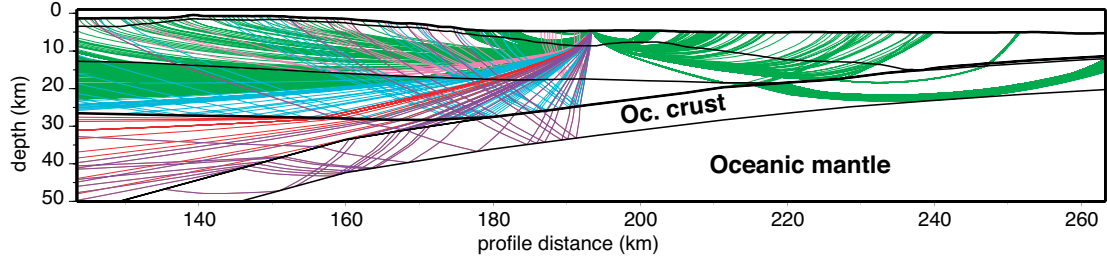
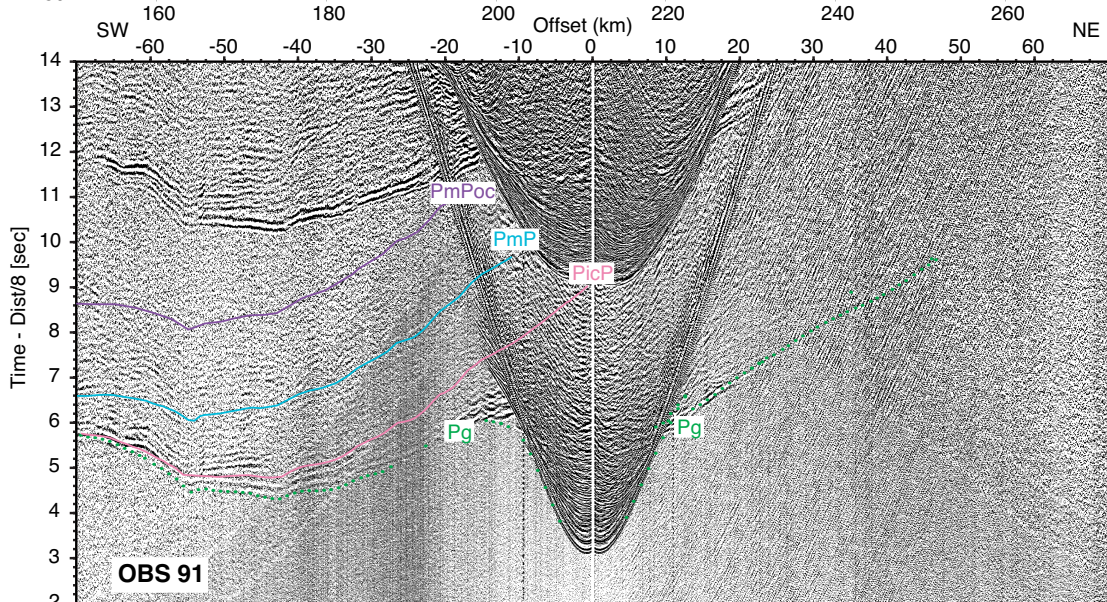
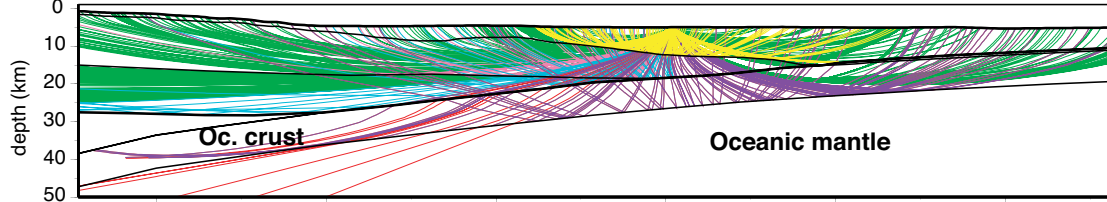
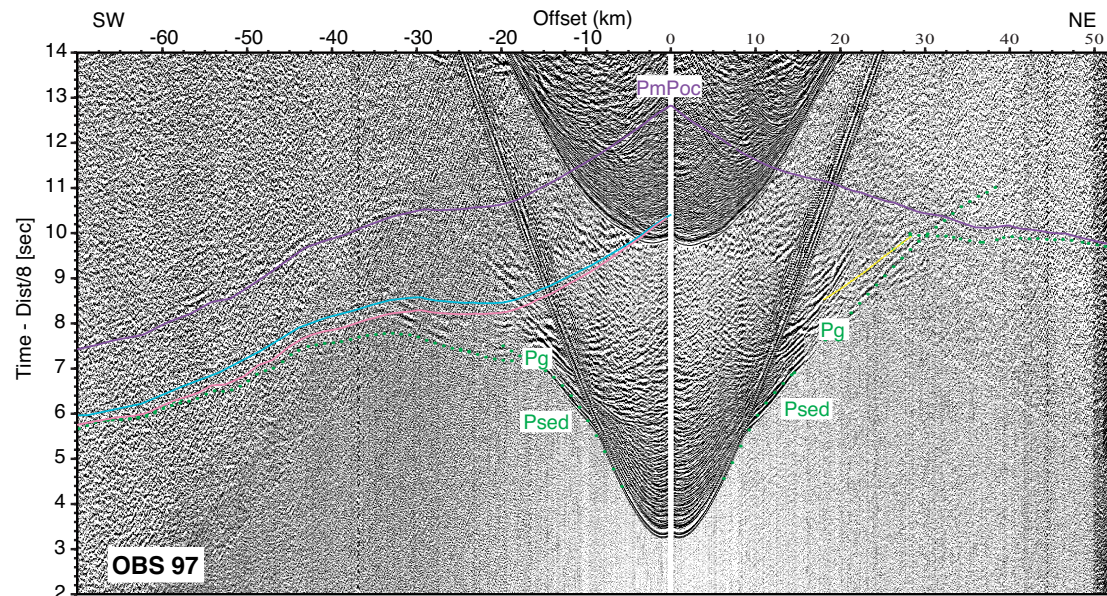
Figure 3.6: Two-dimensional velocity model across the Lesser Antilles island arc achieved by ray tracing. The refraction tomography and pre-stack depth migrated reflection image were used as a priori information in the initial forward model. Layers A-D summarize the geological interpretation of the Caribbean plate crust and upper mantle: A- sediments, volcanics and volcanic rocks compose the upper crust. B- Middle crust of felsic to intermediate composition. C- Lower crust of gabbroic plutons. D- upper mantle. Bottom image displays the derivative weight sum (DWS) of rays through the model.

to the Grenada Basin (Fig. 3.6). Approximately 1900 m of sediment are trapped in the Grenada Basin, however, the basin's eastern margin is only covered by four seismic stations (OBS 61-64) and resolution beyond the instrument layout is limited due to lower ray coverage (Figs. 3.2 and 3.6). Sediments are mainly sourced from the island arc, where a well-developed canyon system provides transport paths to the

basin (Fig. 3.1).

Two distinct island arc crustal layers below the upper volcanogenic sedimentary rock unit are resolved: a middle crust with a velocity gradient of 0.28 s^{-1} and a lower crustal layer with a gradient of 0.038 s^{-1} . The crust-mantle boundary is found at an average depth of 28 km (Fig. 3.6). Upper mantle velocities of 8 km/s are well constrained by reverse shots along the central portion of the island arc beneath the volcanic front (Fig. 3.9). Whereas the crust underneath the Grenada Basin shows a uniform structure at a constant thickness of 23 km; the crustal geometry underneath the island arc is characterized by locally thickened segments. The PicP reflector at the base of the middle crust smoothly bends upwards underneath stations 71 to 82 (Fig. 3.6). As the basement does not follow this trend, the thickening of the lower crust here corresponds to a locally thinned middle crust. The eastern portion of the island arc is characterized by a basement high extending from profile km 130 to 170. Only a thin sediment cover of a few hundred meters and less is resolved over the basement high; sediment thickens towards the volcanic front. The mid-crustal reflection PicP can be traced northeastwards underneath Ridge B.

Figure 3.7 (following page): Seismic wide-angle sections for OBS 97 and 91 and corresponding ray penetration through the model. See Figure 3.6 for instrument location. Calculated travel times through the forward model displayed in Figure 3.6 are shown as color-coded lines. Reduction velocity is 8 km/s. See Table 1 for phase information. Pg refractions are shown in green; intracrustal as well as PmP reflections of the Caribbean plate are shown in pink and turquoise, respectively. Oceanic basement and PmP reflections are displayed in purple and orange. The yellow arrival traces the forearc basement reflection.



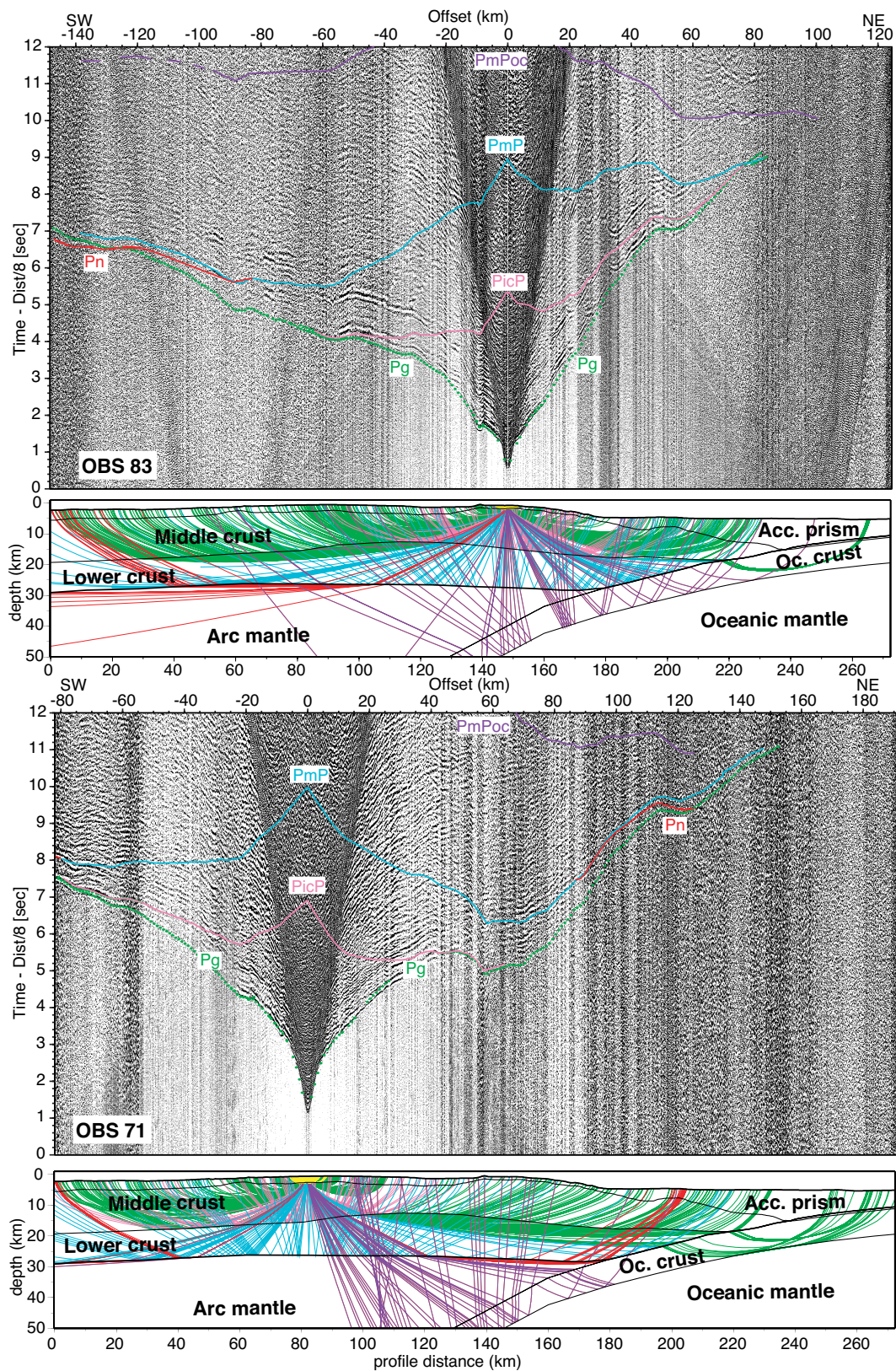


Figure 3.8: Seismic wide-angle sections for OBS 83 and 71 and corresponding ray penetration through the model. See Figure 3.7 caption for display information.

3.7 Discussion and conclusions

3.7.1 Oceanic Domain

Due to the thick accumulation of sediment on top of the incoming North American oceanic crust, seismic energy penetration along our profile is not sufficient to resolve the velocity structure of the oceanic mantle. Low upper mantle velocities (~ 7.5 – 7.8 km/s) have been documented for a number of subduction zones globally and have been attributed to highly fractured crust facilitating mantle hydration processes (e.g. Faccenda et al., 2009; Planert et al., 2010). The oceanic basement is well resolved along a ~ 50 km segment by our forward model (220–270 km offset), where there is little indication for considerable basement relief related to deeply penetrating normal faults (Fig. 3.4). Convergent margins displaying a thick sedimentary blanket are less prone to hydration processes than margins where permeable basement rock is widely exposed on the seafloor. Here, water may enter the igneous crust along outcropping basement highs or tectonic faults breaching the seafloor (Faccenda et al., 2009). The thick sedimentary cover characteristic for the Lesser Antilles margin likely inhibits ocean-basement interaction and hinders penetration of seawater into the crust and mantle. The structure and seismic velocities of the incoming oceanic crust show typical values for mature, unaltered oceanic crust (Carlson, 1998). We speculate that upper mantle velocities follow this trend and are in the range of 7.9–8.3 km/s associated with an anhydrous condition of peridotite in the upper mantle (Peacock, 1990).

3.7.2 Forearc-island arc transition and backstop topography

The seismic refraction and reflection grid of Bangs et al. (2003) and Christeson et al. (2003) reveals a laterally undulating topography of Ridge A, which is also imaged in our reflection profile (Fig. 3.4) and could be an indication that the relief originates from crustal fragments that would be easier to accrete than a continuously developed aseismic ridge. Ridge B is also well recovered along our profile (Figs. 3.2, 3.4, and 3.6); its top is traced between offsets of 190–215 km. The line crosses a local peak of

Ridge B (Fig. 3 of Bangs et al., 2003), where it reaches a depth of 8 km.

The seaward dipping geometry of the backstop resembles the backstop structure found offshore southern Sumatra and western Java. Frontal accretion dominates along this central segment of the Sunda margin (Kopp et al., 2009) and a dual backstop structure controls material transfer processes and the evolution of the accretionary prism here (Kopp et al., 2001, 2002). However, compared to the central Lesser Antilles, the backstop along the central Sunda margin is characterized by a much more subdued, uniform geometry without distinct ridges and troughs as imaged offshore Guadeloupe. This may be an artifact resulting from the 2D seismic coverage along Sunda (Kopp and Kukowski, 2003) compared to the three-dimensional imaging of the Lesser Antilles (Christeson et al., 2003). Another explanation would be the composite character of the Lesser Antilles backstop as proposed by Bangs et al. (2003), with incorporation of accreted fragments of oceanic crust or aseismic ridges.

A similar basement topography pattern has been documented offshore eastern Java (Shulgin et al., 2010) and has been attributed to accretion of fragments of a buoyant aseismic oceanic plateau. A composition sourced from different units is supported by the segmentation of the arc basement underneath the Ridges A and B (Fig. 3.4), where a steeply landward dipping fault separates two basement blocks. The original backstop fronting the volcanic arc was uplifted to form Ridge B when a second unit arrived (Bangs et al., 2003), which was subsequently deformed as Ridge A evolved. Deformation of a backstop has been documented for the Nankai margin, where a landward indentation of the crustal block of old accreted sediments, which serves as backstop, has been attributed to the subduction of oceanic basement relief (Nakanishi et al., 2002). Intense deformation of the forearc crust is also observed on the Ryukyu margin (Font and Lallemand, 2009). Strong trench-perpendicular compression of the forearc basement concurs with the uplift of a broken piece of Ryukyu arc basement caused by the subduction of oceanic relief. This complex interplay of oceanic basement block subduction and deformation of the upper plate basement thus mirrors the situation along the central Antilles margin.

A broad swell is observed between 130-170 km offset east of the active arc and is associated with a positive gravity anomaly. Sediment thickness here is greatly decreased

compared to the western part of the island arc (Fig. 3.6). This region corresponds to an elongated high observed in the bathymetry data (Fig. 3.1), the Karukera Spur. It extends for approximately 80 km in a NW-SE (160°) direction (Fig. 3.1) and lies in the projected prolongation of the Tiburon Ridge. However, our seismic data do not reveal the subducted ridge, which would be expected at depths exceeding 25 km between OBS 83 and 88 at offsets around ~ 170 km. We can thus only speculate on a possible relation between ridge subduction and forearc uplift. Recent numerical modeling has shown that a stable effect of ridge subduction is an increase in local topography. The net uplift may exceed the height of the subducted seafloor relief due to additional shortening of the overriding plate (Gerya et al., 2009).

3.7.3 Island arc structure

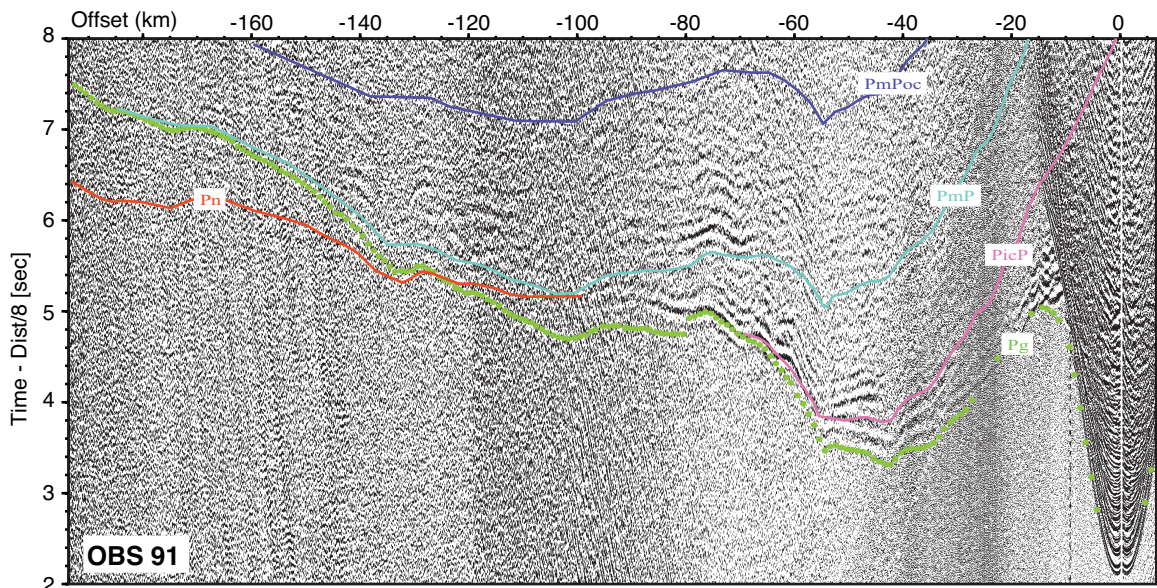
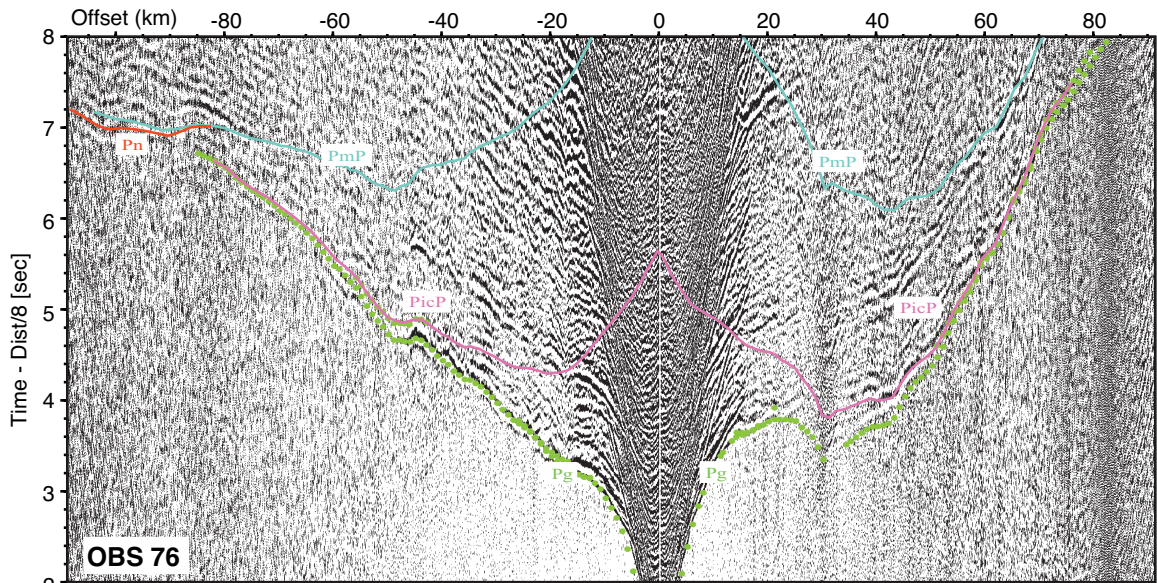
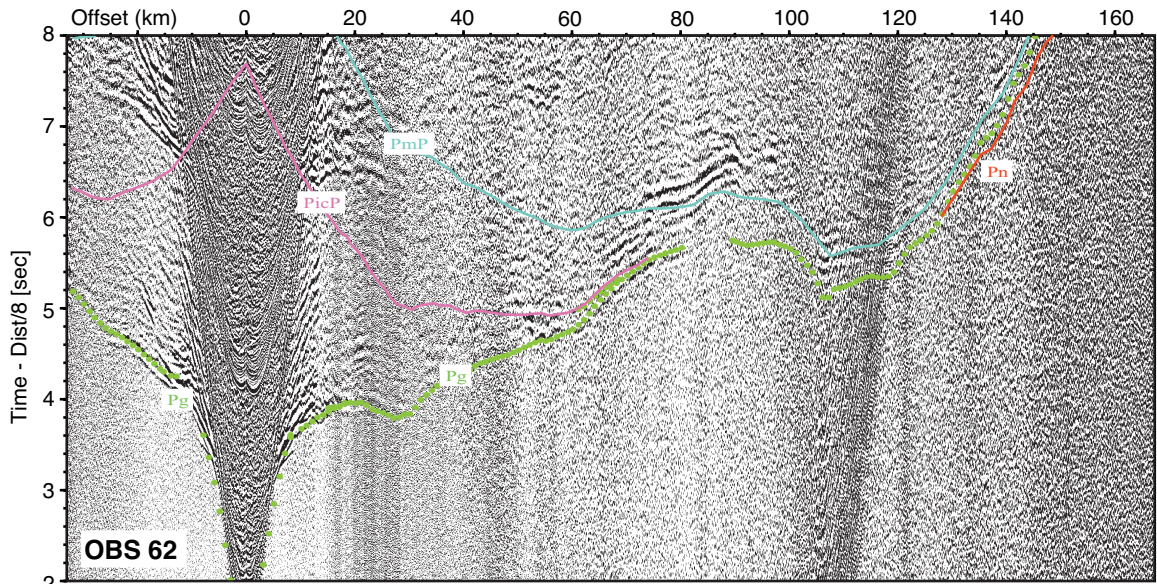
The island arc crust is divided into three layers, with a total average thickness of 23-24 km. These values are compatible with crustal investigations along the southern extent of the Lesser Antilles island arc (TRIN transect; Christeson et al., 2008), which resolved a ~ 24 km thick crust underneath the island arc. The TRIN tomographic inversion of the crust was based on first arrivals and thus did not resolve an intracrustal reflector (Christeson et al., 2008). The seismic velocities retrieved for the island arc in our study are in the range of velocities found along the southern TRIN transect (Christeson et al., 2008). For the Montserrat region (Fig. 3.1), Sevilla et al. (2010) estimate a crustal thickness ranging from 26-34 km based on receiver function analysis. Their velocity-depth distribution identifies similar seismic velocities and provides corroboration for our interpretation of crustal velocities across the island arc. Previous investigations crossing the island arc were mainly based on gravity modeling with only sparse seismic information and slightly overestimated crustal thickness (Westbrook, 1975; Boynton et al., 1979; Maury et al., 1990).

The upper island arc crust along our transect shows little variation in thickness except where the sediment cover characterized by seismic velocities lower than 3.0 km/s is changing (e.g. increasing sediment thickness in the Grenada Basin and decreasing sediment cover across the Karukera Spur) (Fig. 3.6). The 160 km distance from the

active volcanic front to the updip contact of the upper plate crust with the subduction lower plate as identified here by reflection-refraction data is on the order of that reported for other arcs (although the additional distance to the deformation front may vary depending on the extensions of a possible accretionary wedge) (Suyehiro et al., 1996; Holbrook et al., 1999; Lizarralde et al., 2002). The upper crust below the sediment blanket is interpreted to consist mainly of volcanoclastics and intrusive and extrusive igneous rocks with seismic velocities between sedimentary values and 5.5–6.0 km/s. This wide range in upper crustal velocities may be attributed to varying degrees in fluid content, fracturing and porosity and alteration.

The velocity distribution of the forearc middle crust (Figs. 3.2 and 3.6) is in the range of typical continental crust velocities, which show an average velocity of 6.4 ± 0.2 km/s (Christensen and Mooney, 1995; Rudnick and Fountain, 1995). The bulk composition of the middle crust ($v_p < 6.8$ km/s) is interpreted to be felsic to intermediate. This layer is on the order of 10 km thick with velocities increasing from 5.5–6.0 km/s to 6.8 km/s. The survey does not resolve an internal stratigraphy beyond defining a gradient with depth. This results from traveltime modeling of waves traversing it. Because of the variation in bathymetry and heterogeneous shallow cover, there is certainly a difficulty to identify short travel time branches if they existed, that could indicate the internal layering. The bulk volume and thickness of the middle crust is comparable to tomographic images of the Izu arc (Kodaira et al., 2007a) or Mariana arc (Takahashi et al., 2007) and significantly larger than for the Bonin segment (Kodaira et al., 2007b). The active volcanic front is located around stations 67–68 (Fig. 3.6) and is characterized by increased seismic velocities beneath the volcanic centers around 60 km offset. The sediment cover is absent on top of this active zone and the upward bending of the velocity isolines is focused along a narrow

Figure 3.9 (following page): Record sections of stations deployed on the Caribbean plate to analyze the intracrustal boundary between the middle and lower crust as well as the upper plate Moho as displayed in Figure 3.6. Reverse shooting resolves two individual arrivals PicP and Pmp and supports the interpretation of an intracrustal impedance contrast in addition to the crust-mantle boundary. Instrument location is shown in Figure 3.6. See Figure 3.7 caption for further display information.



zone, corresponding to the finite area of active volcanism (Macdonald et al., 2000). A three-dimensional seismic refraction/reflection tomography around Montserrat island (Fig. 3.1) resolved the andesitic cores of the volcanic centers, which are built of andesite lava domes and intrusions with seismic velocities of 3.5 km/s to 5.5 km/s (Shalev et al., 2010; Paulatto et al., 2010).

The plutonic lower crust shows velocities increasing from 7.1 km/s to 7.3 km/s. It is extending throughout the section, over at least 150 km and forms the present lower crustal layer extending from the forearc to the backarc domain. This layer has an average thickness of 12 km with notably only a long-wavelength moderate variation by 20%. A corresponding (though significantly thinner) crustal unit along the Izu-Bonin arc (Kodaira et al., 2007b) is interpreted there as gabbroic plutons. This interpretation could be shared for the Lesser Antilles, however, exposures of these rocks have not been reported for the Lesser Antilles, for which we infer an intermediate composition sourced from differentiation of deeper mafic material. It should be noted, though, that inferring composition from seismic velocity distribution depends on the thermal gradient structure (Shillington et al., 2004). There is no indication of a high density ultramafic cumulates layer as found e.g. along the Izu-Bonin arc (Kodaira et al., 2007b) and central Aleutian arc (Shillington et al., 2004) and upper mantle velocities across the Lesser Antilles island arc are in the range of 8 km/s, with little indication for serpentinization. This observation is relevant with regards to the generation of continental crust: the andesitic bulk composition of continental crust requires differentiation of basaltic melts to form continental crust (McClellan et al., 2008). 'Foundering' or delamination of a lower ultramafic crustal layer has been proposed to occur during the growth of continental crust (e.g. Kay and Mahlburg Kay, 1988; Kay, 1993; Kelemen et al., 2003). This process requires the crustal section to become convectively unstable and thus be denser than the underlying mantle peridotite, which would concur with P wave velocities exceeding 7.4 km/s (Behn and Kelemen, 2006). The range of lower crust v_p values (6.8-7.3 km/s) observed across the central Lesser Antilles arc along our profile corresponds to seismic observations of the Central Aleutians (Holbrook et al., 1999; Lizarralde et al., 2002), though along strike values there are higher (Fliedner and Klemperer,

1999, 2000; Shillington et al., 2004) as is the case for Izu-Bonin (Suyehiro et al., 1996; Kodaira et al., 2007b). This layer likely represents mafic rocks and intermediate plutons added to the primitive crust on which the Lesser Antilles evolved. Behn and Kelemen (2006) note that seismic P wave velocity alone is an inadequate indicator of major element chemistry and SiO₂ content and compositions ranging from basaltic to dacitic match the corresponding velocities (Behn and Kelemen, 2003). Against this backdrop, the average composition of the central Lesser Antilles arc crust may serve as one component for building continental crust. Delamination or transformation of major crustal units (Kay, 1993), as proposed for the central Aleutians or Izu-Bonin is not required for the Lesser Antilles where a primitive, high density cumulates section (either in the lower crust or upper mantle) is absent.

Numerical modeling suggests that the volume of new-formed crust in island arcs correlates with the age of the subducted slab. In addition, the rate of crust accumulation in the island arc depends on the velocity of plate retreat (Nikolaeva et al., 2008). Thus the dynamics of subduction will influence crustal growth and consequently shape the volume of the island arc. As mentioned earlier, the dimension from forearc to backarc is comparable to other arcs and subduction zones. However, the remarkably uniform crustal thickness spanning the entire section of ~ 200 km across strike is in contrast to other arc settings. Lateral heterogeneity across the central Lesser Antilles island arc, however, is insignificant compared to the tomographic images of e.g. the Izu-Bonin (Ogasawara)-Mariana arc system. Indeed, the beststudied intra-oceanic subduction systems (e.g. Alaska-Aleutian trench, Izu-Bonin (Ogasawara)-Mariana trench system) display a distinct variability along the cross-sections regarding crustal thickness and velocity distribution. Upper plate crustal thickness varies from typical oceanic crust beneath the forearc and backarc through thickened crust underneath the volcanic front (e.g. Suyehiro et al., 1996; Holbrook et al., 1999; Takahashi et al., 2007). This is commonly interpreted as the signature of the focused material advection resulting from arc volcanism. In comparison to these typical examples, there is a reduced importance of volcanic edifices and eruptive production along the Lesser Antilles arc (Macdonald et al., 2000) and hence an expected subdued importance of magmatic advection such as intrusions or roots of cumulates and thickening of the

original oceanic crust or its underplating. In summary, the considerable volume of the present lower crustal unit (if beneath what could have been originally an oceanic crust) is much larger than in sections of intra-oceanic subductions. In addition, it is not focused underneath the volcanic centers but is imaged from the forearc to the backarc regions. This layer may comprise segments of oceanic plateau material of thickened crust (Diebold, 2009). In this view, the Lesser Antilles arc may rest upon a portion of the Caribbean plateau (Mauffret, 1997) with original oceanic crust thickened by deep magmatic processes and underplating prior to the evolution of the Lesser Antilles arc (Diebold, 2009). The present island arc structure as imaged in this survey with a crustal thickness of 25 km may exhibit an inherited structure resulting from the complex history of the original Caribbean crust.

Chapter 4

Conclusions

For the complete analysis of the transect I chose a novel approach. It has been shown by numerous authors that a forward modelling approach with a subsequent tomographic inversion is a powerful way of viewing and retrieving subsurface parameters. In this study, I chose another approach and began with a tomography of first arrivals to define the shallow - and in general well resolved - velocity structure for a consecutive second arrival forward modelling.

In conclusion, the approach I chose has proven that the retrieval of a smooth velocity model, based on first arrivals and its subsequent incorporation in a forward modelling of later arrivals, presents a powerful and effective tool especially for large data sets like the one presented in this thesis. To commence the analysis with forward modeling, as in the conventional approach, is a time consuming and intricate challenge - especially if 50 or more instruments are involved. Furthermore, the tomography allows a detailed estimate of the resolution and gives rise to new considerations such as the validity of the a-priori information used to retrieve a result. On the other hand, it is not very intuitive to deduce a geologic model obtained by forward modelling of later arrivals from a smooth velocity structure. This can either be done in a floating reflector frame inside a smooth model or by reinvestigating the top to bottom layering of the later arrivals. In general, the technique chosen is a trade-off between acquisition parameters, complexity of investigation area, and preferences of the investigator.

My structural model is consistent with results and structural knowledge obtained

in previous investigations, and can be incorporated in the studies on seismic risk assessment for achieving the objectives of the THALES project.

4.1 Methodology

This thesis presents a new way of analyzing a 2-D seismic wide-angle profile. Although often numerically expensive, it is inevitable to address the question of confidence intervals of parameters retrieved by indirect measurements. In this thesis, a Bayesian approach was chosen to deal with this particular question. Mathematically well defined, I was able to reduce parameter uncertainties as well as to develop an approach in the framework of my resolution analysis which proved capable of dissecting long wide-angle profiles for deep crust and upper mantle studies. This divergence analysis resulted in a visualization of geological features and their confidence intervals. This is a clear advantage compared to calculating the mean of an ensemble of Monte Carlo realizations, yielding an oversimplified (smoothed) solution to the inverse problem disregarding any possible geologic boundaries.

4.2 Geology

Although there have been numerous studies in the Antilles subduction complex, the presented profile and the parallel profile to the south, north of Martinique, are the first ones which cross the complete island arc. The structural model reveals the complexity of this region and retrieves a two-layered crust with a total average thickness of 23-24 km for the Caribbean plate.

The backstop structure is observed between profile kilometers 190 and 220 and shows a seaward dipping geometry. In accordance with the ridge interpretations of Christeson et al. (2003), I was able to associate the structure to ridge B.

The thick accumulation of sediment on top of the incoming North American oceanic crust causes strong energy attenuation and makes it difficult to resolve the velocity structure of the oceanic mantle. There is no considerable basement relief which would be an indicator of deeply penetrating normal faults. The approximately 80 Ma old

Atlantic plate has an average thickness of 8 km and shows a dip angle of 14° .

4.2.1 Seismogenic zone and rupture area

The work of Fuller et al. (2006) as well as of Byrne et al. (1988) have demonstrated that the updip limit of plate boundary seismicity might coincide with the backstop location. The observations of Wang and Hu (2006) conclude that the actively deforming outer wedge overlies the updip velocity-strengthening portion, while the downdip limit of the seismogenic zone can be vertically associated with the stable inner wedge. The downdip extent of the seismogenic zone on subduction thrusts reaches up to the 300° - 350° C (Tichelaar and Ruff, 1993) isotherm, and the observations from Ruff and Tichelaar (1996) have shown that modern coastlines could be a geomorphological indicator of the downdip limit of the seismic rupture in many subduction zones. Although this observation may be accurate for other island arcs, like the Aleutians, I used the interplate interface to constrain the extent and depth

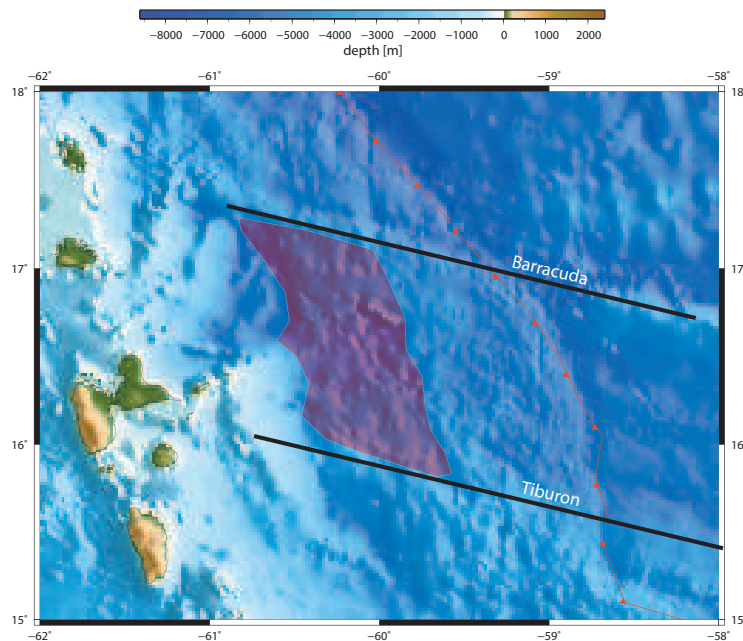


Figure 4.1: Potential rupture area bounded to North and South by the Barracuda and Tiburon Ridge respectively.

of the seismogenic zone. Analyzing my final model accordingly we have a possible seismogenic zone with a width of $\sim 50-60$ km and reaching a depth of ~ 30 km. This result is consistent with previous observations and supports those made by Tichelaar and Ruff (1993), Fuller et al. (2006), and Gutscher et al. (2009).

Seamounts or ridges can influence the size of maximum slip regions and asperities. As found in the Nankai trough by Kodaira et al. (2000), ridges can act as barriers to seismic rupture and therefore limit the total area of failure. The controlled influence of seafloor roughness on the earthquake rupture behaviour has been studied for example by Bilek et al. (2003), Obara et al. (2004), Bangs et al. (2006). Kodaira et al. (2002) found weak interplate coupling by a seamount in the Nankai region and concluded that the seismic ruptures can be blocked - both at and in the wake of a seamount. The moderate plate coupling in the vicinity of the buoyant Cocos Ridge localizes seismicity offshore of Costa Rica (Bilek et al., 2003) and is another example of seismological segmentation of a subduction zone.

The tectonic setting of the central Lesser Antilles suggests a limitation of the failure area between the Tiburon and Barracuda ridges. If the downdip limit of the seismogenic zone is prolonged in a North-South direction along the forearc high and the slope break seen in the bathymetry (Krabbenhöft et al., 2010), which represents an estimate for the updip limit, it is possible to calculate the total rupture area between the subducting ridges (see Fig. 4.1).

Applying the formula of Anderson et al. (1996):

$$M_W = 5.12 + 1.16 \log L - 0.2 \log S$$

with the length of fault rupture L and fault slip rate S , it is possible to determine the magnitude of the earthquake. Let $L \approx 200\text{km}$ denote the N-S extension between the Tiburon and Barracuda ridge and $S \approx 20\text{mm/yr}$ be equal to the plate motion in Figure 1.3. This yields a possible M_W 7.5 event.

Using the regression formula of Wells and Coppersmith (1994):

$$M = 4.07 + 0.98 \log RA$$

with the rupture area RA, with a downdip and updip extent of a rupture of ~ 30 km and ~ 10 km below seafloor, respectively, and a length of ~ 200 km, we have a 200×20 km rupture surface. With a slip rate deficit of 11 mmyr^{-1} from geodetic measurements (Manaker et al., 2008), over a 200 yr recurrence period, it is possible to generate an M_W 7.6 event between 15° - 17° N.

4.3 Outlook

In which way does this work contribute to the objectives of the THALES project? The methods derived from this study are able to consistently retrieve a structure of the contact zone between the overriding and subducting plates. Comparing the MCS lines with the results obtained in the first arrival tomography adds information to the interpretation strategies utilized.

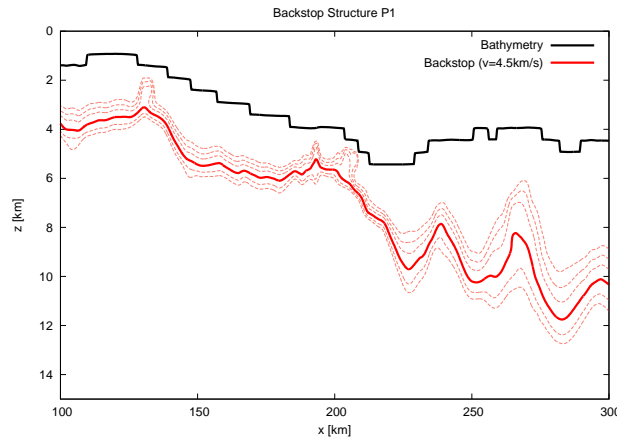


Figure 4.2: Backstop structure along profile P1 of the Merian cruise according to a velocity analysis proposed by Christeson et al. (2003). The thick red curve denotes the backstop.

In the framework of the THALES project, extensive 3-D studies along the convergent margin have been performed (G. Bayrakci, M. Evain personal communication, 2010). Although the models developed by the 3-D analysis of the active seismics acquired may not allow a resolution analysis, i.e. the a priori parameter space was not sampled,

it is possible to use the divergence analysis to decompose the plane of the backstop by filtering and interpolation. Figure 4.2 shows a possible backstop structure according to the interpretation of Christeson et al. (2003).

For further studies, a possible aim could be a divergence analysis on the full 3-D grid which is covered by MCS data, and furthermore to compare the planes for different velocity gradients of predefined distributions to search similarities and redefine the gradients based on the results found. This iterative procedure would offer a novel approach to deduce shallow geological boundaries seen in the near-vertical data by first arrival tomography. In a second step, one could use the results obtained from the updated gradients to search for a specific feature in the complete model, which could result in a better estimate than interpolating between the lines.

Principal component decomposition of the results obtained by the divergence analysis would be a further extension to the plane retrieval, specifically in the domain of sparse ray coverage (Figure 4.3). Not only would this allow to reduce the complex data set to a lower dimension, but it would also be able to create a reference frame for moving on the defined structure.

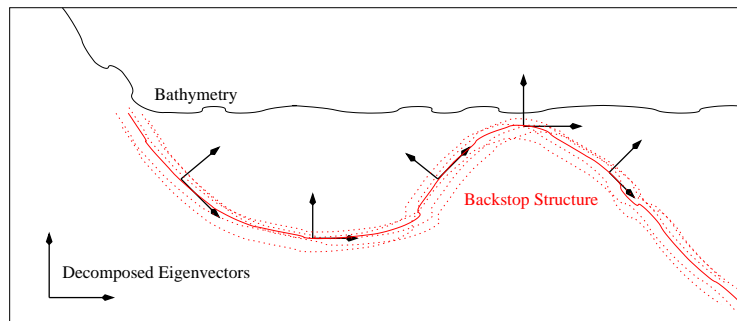


Figure 4.3: Schematic view of the backstop structure and possible analysis of geometry on the basis of Eigenvector decomposition. The principal components at each x-node, with a possible limitation by structural information of surrounding neighbor nodes, can enhance the interpretation in sparsely covered areas.

One of the major objectives of the THALES project is the mapping of the location, size, and spatial variation of the seismogenic megathrust fault. In this context the

structural evolution of the outer and inner wedge of the accretionary domain play a vital role. As has been demonstrated in the work of Kopp and Kukowski (2003) the backstop geometry and composition has a large impact on the accretionary mechanics. While Wang and Hu (2006) extended the classical Coulomb wedge theory and found a correlation between the less deformed inner wedge and updip limit of the seismogenic zone, Fuller et al. (2006) concluded that the seismic coupling correlates with the forearc basins. The transitional segment between a crystalline backstop structure and deformable wedge are subject to erosional and accretionary processes which certainly influence the interplate coupling. The dense acquisition of near-vertical and wide-angle data in the Lesser Antilles offers a unique opportunity for testing the different theories on seismic coupling. The impact of ridge subduction as well as the structural evolution of the geomorphological features arising from this allow an analysis of forearc evolution from North to South. Detailed studies of the backstop geometry will give a better understanding of the evolution of the margin. The formation and deformation of the forearc basins will provide new insights to inner wedge deformation and seismic coupling beneath the stable regions of the subduction wedge. One of the major efforts in the THALES project is the compilation of results. In this regard, the profile presented in this thesis fills a gap which also provides a concept for future investigations. In addition, the structural interpretation offered in this thesis can be used as a basis for deeper studies. Concluding, the Lesser Antilles convergent margin has been imaged in depth and the results obtained may now be used to determine new strategic goals for future mappings of subduction zones.

Bibliography

- Acocella, V., and F. Funiciello, 2010, Kinematic setting and structural control of arc volcanism: *Earth and Planetary Science Letters*, **289**, 43–53.
- Adamek, S., C. Frohlich, and W. D. Pennington, 1988, Seismicity of the Caribbean-Nazca boundary: Constraints on microplate tectonics of the Panama region: *Journal of Geophysical Research*, **93**, 2053–2075.
- Anderson, J. G., S. G. Wesnousky, and M. W. Stirling, 1996, Earthquake Size as a Function of Fault Slip Rate: *Bulletin of the Seismological Society of America*, **86**, 683–690.
- Bangs, N. L., G. L. Christeson, and T. H. Shipley, 2003, Structure of the Lesser Antilles subduction zone backstop and its role in a large accretionary system: *Journal of Geophysical Research (Solid Earth)*, **108**, 2358.
- Bangs, N. L. B., S. P. S. Gulick, and T. H. Shipley, 2006, Seamount subduction erosion in the Nankai Trough and its potential impact on the seismogenic zone: *Geology*, **34**, 701.
- Bangs, N. L. B., and G. K. Westbrook, 1991, Seismic modeling of the decollement zone at the base of the Barbados Ridge accretionary complex: *Journal of Geophysical Research*, **96**, 3853–3866.
- Bangs, N. L. B., G. K. Westbrook, J. W. Ladd, and P. Buhl, 1990, Seismic velocities from the Barbados Ridge complex: Indicators of high pore fluid pressures in an accretionary complex: *Journal of Geophysical Research*, **95**, 8767–8782.
- Behn, M. D., and P. B. Kelemen, 2003, Relationship between seismic P-wave velocity and the composition of anhydrous igneous and meta-igneous rocks: *Geochemistry, Geophysics, Geosystems*, 1.

- Behn, M. D., and P. B. Kelemen, 2006, Stability of arc lower crust: Insights from the Talkeetna arc section, south central Alaska, and the seismic structure of modern arcs: *Journal of Geophysical Research (Solid Earth)*, **111**, 11207.
- Bilek, S. L., S. Y. Schwartz, and H. R. Deshon, 2003, Control of seafloor roughness on earthquake rupture behavior: *Geology*, **31**, 455.
- Bouysse, P., 1988, Opening of the Grenada back-arc Basin and evolution of the Caribbean plate during the Mesozoic and early Paleogene: *Tectonophysics*, **149**, 121–143.
- Bouysse, P., 1990, Subduction of Atlantic aseismic ridges and Late Cenozoic evolution of the Lesser Antilles island arc: *Tectonophysics*, **175**, 349–355.
- Bouysse, P., and D. Westercamp, 1990, Subduction of Atlantic aseismic ridges and Late Cenozoic evolution of the Lesser Antilles island arc: *Tectonophysics*, **175**, 349–380.
- Bowin, C., 1976, Caribbean gravity field and plate tectonics: Boulder, Colo.: Geological Society of America.
- Boynnton, C. H., G. K. Westbrook, M. H. P. Bott, and R. E. Long, 1979, A seismic refraction investigation of crustal structure beneath the Lesser Antilles island arc: *Geophysical Journal International*, **58**, 371–393.
- Brace, W. F., and J. D. Byerlee, 1966, Stick-Slip as a Mechanism for Earthquakes: *Science*, **153**, 990–992.
- Brun, R., and F. Rademakers, 1997, ROOT - An object oriented data analysis framework: *Nuclear Instruments and Methods in Physics Research A*, **389**, 81–86.
- Byrne, D. E., D. M. Davis, and L. R. Sykes, 1988, Loci and maximum size of thrust earthquakes and the mechanics of the shallow region of subduction zones: *Tectonics*, **7**, 833–857.
- Carlson, R. L., 1998, Seismic velocities in the uppermost oceanic crust: Age dependence and the fate of layer 2A: *Journal of Geophysical Research*, **103**, 7069–7078.
- Christensen, N. I., and W. D. Mooney, 1995, Seismic velocity structure and composition of the continental crust: A global view: *Journal of Geophysical Research*, **100**, 9761–9788.
- Christeson, G. L., N. L. Bangs, and T. H. Shipley, 2003, Deep structure of an island

- arc backstop, Lesser Antilles subduction zone: *Journal of Geophysical Research (Solid Earth)*, **108**, 2327.
- Christeson, G. L., P. Mann, A. Escalona, and T. J. Aitken, 2008, Crustal structure of the Caribbean-northeastern South America arc-continent collision zone: *Journal of Geophysical Research (Solid Earth)*, **113**, 8104.
- Clift, P., and P. Vannucchi, 2004, Controls on tectonic accretion versus erosion in subduction zones: Implications for the origin and recycling of the continental crust: *Reviews of Geophysics*, **42**, 2001.
- Collot, J., and M. A. Fisher, 1989, Formation of forearc basins by collision between seamounts and accretionary wedges: An example from the New Hebrides subduction zone: *Geology*, **17**, 930.
- Dahlen, F. A., J. Suppe, and D. Davis, 1984, Mechanics of fold-and-thrust belts and accretionary wedges Cohesive Coulomb theory: *Journal of Geophysical Research*, **89**, 10087–10101.
- Davidson, J. P., and R. J. Arculus, 2008, *in* The significance of Phanerozoic arc magmatism in generating continental crust: 135–172.
- Davis, D., J. Suppe, and F. A. Dahlen, 1983, Mechanics of fold-and-thrust belts and accretionary wedges: *Journal of Geophysical Research*, **88**, 1153–1172.
- DeMets, C., P. E. Jansma, G. S. Mattioli, T. H. Dixon, F. Farina, R. Bilham, E. Calais, and P. Mann, 2000, GPS geodetic constraints on Caribbean-North America plate motion: *Geophysical Research Letters*, **27**, 437.
- Diebold, J., 2009, Submarine volcanic stratigraphy and the Caribbean LIP's formational environment: *Geological Society London, Spec. Pub.*, **328**, 799–808.
- Faccenda, M., T. V. Gerya, and L. Burlini, 2009, Deep slab hydration induced by bending-related variations in tectonic pressure: *Nature Geoscience*, **2**, 790–793.
- Feuillet, N., 2000, Sismotectonique des Petites Antilles: PhD thesis, Univ. Paris VII-Denis Diderot Univ.
- Feuillet, N., I. Manighetti, P. Tapponnier, and E. Jacques, 2002, Arc parallel extension and localization of volcanic complexes in Guadeloupe, Lesser Antilles: *Journal of Geophysical Research (Solid Earth)*, **107**, 3–1.
- Fliedner, M. M., and S. L. Klemperer, 1999, Structure of an island-arc: Wide-angle

- seismic studies in the eastern Aleutian Islands, Alaska: *Journal of Geophysical Research*, **104**, 10667–10694.
- Fliedner, M. M., and S. L. Klemperer, 2000, Crustal structure transition from oceanic arc to continental arc, eastern Aleutian Islands and Alaska Peninsula: *Earth and Planetary Science Letters*, **179**, 567–579.
- Flinch, J. F., et al., 1999, Structure of the Gulf of Paria pull-apart Basin (Eastern Venezuela-Trinidad): In: P. Mann (Editor), *Caribbean Basins. Sedimentary Basins of the World*, 477–494.
- Font, Y., and S. Lallemand, 2009, Subducting oceanic high causes compressional faulting in southernmost Ryukyu forearc as revealed by hypocentral determinations of earthquakes and reflection/refraction seismic data: *Tectonophysics*, **466**, 255–267.
- Fuller, C. W., S. D. Willett, and M. T. Brandon, 2006, Formation of forearc basins and their influence on subduction zone earthquakes: *Geology*, **34**, 65.
- Gerya, T. V., D. Fossati, C. Cantieni, and D. Seward, 2009, Dynamic effects of aseismic ridge subduction: numerical modeling: *European Journal of Mineralogy*, **21**, 649–661.
- Gutscher, M., G. K. Westbrook, B. Marcaillou, D. Graindorge, A. Gailler, T. Pichot, and R. Maury, 2009, How wide is the seismogenic zone of the Lesser Antilles forearc?: AGU Fall Meeting Abstracts, D8+.
- Gutscher, M. A., and G. K. Westbrook, 2009, *in* *Great Earthquakes in Slow-Subduction, Low-Taper Margins*: Springer, 119.
- Hansen, T. M., A. G. Journel, A. Tarantola, and K. Mosegaard, 2006, Linear inverse Gaussian theory and geostatistics: *Geophysics*, **71**, 101.
- Heubeck, C., and P. Mann, 1991, Geologic evaluation of plate kinematic models for the northern Caribbean plate boundary zone: *Tectonophysics*, **191**, 1–26.
- Hjelt, S., 1992, *Pragmatic Inversion of Geophysical Data: Lecture Notes in Earth Sciences*, Berlin Springer Verlag, **39**.
- Holbrook, W. S., D. Lizarralde, S. McGeary, N. Bangs, and J. Diebold, 1999, Structure and composition of the Aleutian island arc and implications for continental crustal growth: *Geology*, **27**, 31.

- Holcombe, T. L., et al., 1990, Caribbean marine geology: Ridges and basins of the plate interior.
- Huang, J., E. Vanacore, F. Niu, and A. Levander, 2010, Mantle transition zone beneath the Caribbean-South American plate boundary and its tectonic implications: *Earth and Planetary Science Letters*, **289**, 105–111.
- Hyndman, R. D., and K. Wang, 1993, Thermal constraints on the zone of major thrust earthquake failure - The Cascadia subduction zone: *Journal of Geophysical Research*, **98**, 2039–2060.
- Ida, Y., 1975, Analysis of stick-slip and earthquake mechanism: *Physics of the Earth and Planetary Interiors*, **11**, 147–156.
- Jacobsen, B. H., K. Mosegaard, and P. Sibani, 1996a, *Inverse Methods*: Springer-Verlag Berlin Heidelberg New York.
- Jacobsen, B. H., K. Mosegaard, and P. Sibani, 1996b, *Inverse Methods. Interdisciplinary Elements of Methodology, Computation, and Applications*: Springer-Verlag Berlin Heidelberg New York.
- James, F., and M. Roos, 1975, Minuit - a system for function minimization and analysis of the parameter errors and correlations: *Computer Physics Communications*, **10**, 343–367.
- Jordan, T. H., 1975, The present-day motions of the Caribbean plate: *Journal of Geophysical Research*, **80**, 4433–4439.
- Kato, N., and T. Hirasawa, 1999, Nonuniform and Unsteady Sliding of a Plate Boundary in a Great Earthquake Cycle: A Numerical Simulation Using a Laboratory-derived Friction Law: *Pure and Applied Geophysics*, **155**, 93–118.
- Kay, R., 1993, Delamination and delamination magmatism: *Tectonophysics*, **219**, 177–189.
- Kay, R. W., and S. Mahlburg Kay, 1988, Crustal recycling and the Aleutian arc: *Geochimica et Cosmochimica Acta*, **52**, 1351–1359.
- Kelemen, P. B., K. Hanghøj, and A. R. Greene, 2003, One View of the Geochemistry of Subduction-related Magmatic Arcs, with an Emphasis on Primitive Andesite and Lower Crust: *Treatise on Geochemistry*, **3**, 593–659.
- Kirsch, A., 1996, *An introduction to the mathematical theory of inverse problems*:

- Springer-Verlag New York, Inc.
- Kodaira, S., E. Kurashimo, J. Park, N. Takahashi, A. Nakanishi, S. Miura, T. Iwasaki, N. Hirata, K. Ito, and Y. Kaneda, 2002, Structural factors controlling the rupture process of a megathrust earthquake at the Nankai trough seismogenic zone: *Geophysical Journal International*, **149**, 815–835.
- Kodaira, S., T. Sato, N. Takahashi, A. Ito, Y. Tamura, Y. Tatsumi, and Y. Kaneda, 2007a, Seismological evidence for variable growth of crust along the Izu intraoceanic arc: *Journal of Geophysical Research (Solid Earth)*, **112**, 5104.
- Kodaira, S., T. Sato, N. Takahashi, S. Miura, Y. Tamura, Y. Tatsumi, and Y. Kaneda, 2007b, New seismological constraints on growth of continental crust in the Izu-Bonin intra-oceanic arc: *Geology*, **35**, 1031.
- Kodaira, S., T. Sato, N. Takahashi, M. Yamashita, T. No, and Y. Kaneda, 2008, Seismic imaging of a possible paleoarc in the Izu-Bonin intraoceanic arc and its implications for arc evolution processes: *Geochemistry, Geophysics, Geosystems*, **9**, 10.
- Kodaira, S., N. Takahashi, A. Nakanishi, S. Miura, and Y. Kaneda, 2000, Subducted Seamount Imaged in the Rupture Zone of the 1946 Nankaido Earthquake: *Science*, **289**, 104–106.
- Kopp, H., E. R. Flueh, D. Klaeschen, J. Bialas, and C. Reichert, 2001, Crustal structure of the central Sunda margin at the onset of oblique subduction: *Geophysical Journal International*, **147**, 449–474.
- Kopp, H., D. Hindle, D. Klaeschen, O. Oncken, C. Reichert, and D. Scholl, 2009, Anatomy of the western Java plate interface from depth-migrated seismic images: *Earth and Planetary Science Letters*, **288**, 399–407.
- Kopp, H., D. Klaeschen, E. R. Flueh, J. Bialas, and C. Reichert, 2002, Crustal structure of the Java margin from seismic wide-angle and multichannel reflection data: *Journal of Geophysical Research (Solid Earth)*, **107**, 2034.
- Kopp, H., and N. Kukowski, 2003, Backstop geometry and accretionary mechanics of the Sunda margin: *Tectonics*, **22**, 060000–1.
- Korenaga, J., W. S. Holbrook, G. M. Kent, P. B. Kelemen, R. S. Detrick, H.-C. Larsen, J. R. Hopper, and T. Dahl-Jensen, 2000, Crustal structure of the southeast

- Greenland margin from joint refraction and reflection seismic tomography: *Journal of Geophysical Research*, **105**, 21591–21614.
- Krabbenhöft, A., W. Weinrebe, H. Kopp, E. R. Flueh, S. Ladage, C. Papenberg, L. Planert, and Y. Djajadihardja, 2010, Bathymetry of the Indonesian Sunda margin relating morphological features of the upper plate slopes to the location and extent of. (Submitted to *Earth System Sciences*).
- Laigle, M., E. Roux, M. Sapin, A. Hirn, B. de Voogd, P. Charvis, Y. Hello, Y. Murai, Y. Nishimura, H. Shimamura, A. Galve, J. Lepine, J. Lebrun, J. Diaz, J. Gallart, F. Beauducel, and J. Viode, 2005, Elements of the Seismic Structure and Activity of the Lesser Antilles Subduction Zone (Guadeloupe and Martinique Islands) from the SISMANTILLES Seismic Survey: AGU Fall Meeting Abstracts, C580+.
- Lizarralde, D., W. S. Holbrook, S. McGeary, N. L. Bangs, and J. B. Diebold, 2002, Crustal construction of a volcanic arc, wide-angle seismic results from the western Alaska Peninsula: *Journal of Geophysical Research (Solid Earth)*, **107**, 2164.
- Macdonald, R., C. J. Hawkesworth, and E. Heath, 2000, The Lesser Antilles volcanic chain: a study in arc magmatism: *Earth Science Reviews*, **49**, 1–76.
- Manaker, D. M., E. Calais, A. M. Freed, S. T. Ali, P. Przybylski, G. Mattioli, P. Jansma, C. Prépetit, and J. B. de Chabaliere, 2008, Interseismic Plate coupling and strain partitioning in the Northeastern Caribbean: *Geophysical Journal International*, **174**, 889–903.
- Mann, P., et al., 1995, Actively evolving microplate formation by oblique collision and sideways motion along strike-slip faults: An example from the northeastern Caribbean plate margin: *Tectonophysics*, **246**, 1–69.
- Masclé, A., and A. Letouzey, 1990, Geological Map of the Caribbean.
- Matarese, J., 1993, Nonlinear Traveltime Tomography: PhD thesis, Mass. Inst. of Technol.
- Mauffret, A., 1997, Seismic stratigraphy and structure of the Caribbean igneous province: *Tectonophysics*, **283**, 61–104.
- Maury, R. C., G. K. Westbrook, P. E. Baker, and P. Bouysse, 1990, *in* Geology of the Lesser-Antilles: Geological Society of America, 141–166.

- McClelland, S. M., S. R. Taylor, and S. R. Hemming, 2008, *in* Composition, differentiation, and evolution of the continental crust: Constraints from sedimentary rocks and heat flow: 92–134.
- Mosegaard, K., and M. Sambridge, 2002, TOPICAL REVIEW: Monte Carlo analysis of inverse problems: *Inverse Problems*, **18**, 29.
- Mosegaard, K., and A. Tarantola, 1995, Monte Carlo sampling of solutions to inverse problems: *Journal of Geophysical Research*, **100**, 12431–12448.
- Nakanishi, A., S. Kodaira, J. Park, and Y. Kaneda, 2002, Deformable backstop as seaward end of coseismic slip in the Nankai Trough seismogenic zone: *Earth and Planetary Science Letters*, **203**, 255–263.
- Nikolaeva, K., T. V. Gerya, and J. A. D. Connolly, 2008, Numerical modelling of crustal growth in intraoceanic volcanic arcs: *Physics of the Earth and Planetary Interiors*, **171**, 336–356.
- Nishizawa, A., K. Kaneda, N. Watanabe, and M. Oikawa, 2009, Seismic structure of the subducting seamounts on the trench axis: Erimo Seamount and Daiichi-Kashima Seamount, northern and southern ends of the Japan Trench: *Earth, Planets, and Space*, **61**.
- Obara, K., Y. Haryu, Y. Ito, and K. Shiomi, 2004, Low frequency events occurred during the sequence of aftershock activity of the 2003 Tokachi-Oki earthquake; a dynamic process of the tectonic erosion by subducted seamount: *Earth, Planets, and Space*, **56**, 347–351.
- Parker, R., 1994, *Geophysical Inverse Theory*: Princeton Univ. Press.
- Parker, R. L., and A. M. Dziewonski, 1995, *Geophysical Inverse Theory: Physics Today*, **48**, 92.
- Paulatto, M., T. A. Minshull, B. Baptie, S. Dean, J. O. S. Hammond, T. Henstock, C. L. Kenedi, E. J. Kiddle, P. Malin, C. Peirce, G. Ryan, E. Shalev, R. S. J. Sparks, and B. Voight, 2010, Upper crustal structure of an active volcano from refraction/reflection tomography, Montserrat, Lesser Antilles: *Geophysical Journal International*, **180**, 685–696.
- Peacock, S. M., 1990, Fluid Processes in Subduction Zones: *Science*, **248**, 329–337.
- Planert, L., H. Kopp, E. Lueschen, C. Mueller, E. R. Flueh, A. Shulgin, and Y.

- Djajadihardja, 2010, Lower plate structure and upper plate deformational segmentation at the Sunda-Banda arc transition, Indonesia, resolved from the analysis of seismic and gravity data: *Journal of Geophysical Research*. (in press).
- Press, F., 1968, Earth Models Obtained by Monte Carlo Inversion: *Journal of Geophysical Research*, **73**, 5223.
- Press, F., 1971, *in* An Introduction to Earth Structure and Seismotectonics: *Proc. of the Int. Sch. Phys. Enrico Fermi*, 209.
- Ranero, C. R., I. Grevemeyer, H. Sahling, U. Barckhausen, C. Hensen, K. Wallmann, W. Weinrebe, P. Vannucchi, R. von Huene, and K. McIntosh, 2008, Hydrogeological system of erosional convergent margins and its influence on tectonics and interplate seismogenesis: *Geochemistry, Geophysics, Geosystems*, **9**, 3.
- Roux, E., 2007, Reconnaissance de la Structure Sismique de la Zone de Subduction des Petites Antilles (Guadeloupe et Martinique): PhD thesis, Univ. Paris VII-Denis Diderot Univ.
- Rudnick, R. L., and D. M. Fountain, 1995, Nature and composition of the continental crust: A lower crustal perspective: *Reviews of Geophysics*, **33**, 267–310.
- Ruff, L., and B. Tichelaar, 1996, What controls the seismogenic plate interface in subduction zones?
- Saffer, D. M., and C. Marone, 2003, Comparison of smectite- and illite-rich gouge frictional properties: application to the updip limit of the seismogenic zone along subduction megathrusts: *Earth and Planetary Science Letters*, **215**, 219–235.
- Sambridge, M., and K. Mosegaard, 2002, MONTE CARLO METHODS IN GEOPHYSICAL INVERSE PROBLEMS: *Reviews of Geophysics*, **40**, 1009.
- Sato, T., and B. L. N. Kennett, 2000, Two-dimensional inversion of refraction travel-times by progressive model development: *Geophysical Journal International*, **140**, 543–558.
- Sevilla, W. I., C. J. Ammon, B. Voight, and S. De Angelis, 2010, Crustal structure beneath the Montserrat region of the Lesser Antilles island arc: *Geochemistry, Geophysics, Geosystems*, **11**, 6013.
- Shalev, E., C. L. Kenedi, P. Malin, V. Voight, V. Miller, D. Hidayat, R. S. J. Sparks,

- T. Minshull, M. Paulatto, L. Brown, and G. Mattioli, 2010, Three-dimensional seismic velocity tomography of Montserrat from the SEA-CALIPSO offshore/onshore experiment: *Geophysical Research Letters*, **37**, 0.
- Shillington, D. J., H. J. A. Van Avendonk, W. S. Holbrook, P. B. Kelemen, and M. J. Hornbach, 2004, Composition and structure of the central Aleutian island arc from arc-parallel wide-angle seismic data: *Geochemistry, Geophysics, Geosystems*, **5**, 6.
- Shulgin, A., H. Kopp, C. Mueller, L. Planert, E. Lueschen, E. R. Flueh, and Y. Djajidhardja, 2010, Structural architecture of oceanic plateau subduction offshore Eastern Java and the potential implications for geohazards. (Submitted to *Geophysical Journal International*).
- Stern, R. J., 2002, Subduction Zones: *Reviews of Geophysics*, **40**, 1012.
- Suyehiro, K., N. Takahashi, Y. Ariie, Y. Yokoi, R. Hino, M. Shinohara, T. Kanazawa, N. Hirata, H. Tokuyama, and A. Taira, 1996, Continental Crust, Crustal Underplating, and Low-Q Upper Mantle Beneath an Oceanic Island Arc: *Science*, **272**, 390–392.
- Takahashi, N., S. Kodaira, S. L. Klemperer, Y. Tatsumi, Y. Kaneda, and K. Suyehiro, 2007, Crustal structure and evolution of the Mariana intra-oceanic island arc: *Geology*, **35**, 203.
- Takahashi, N., S. Kodaira, Y. Tatsumi, M. Yamashita, T. Sato, Y. Kaiho, S. Miura, T. No, K. Takizawa, and Y. Kaneda, 2009, Structural variations of arc crusts and rifted margins in the southern Izu-Ogasawara arc-back arc system: *Geochemistry, Geophysics, Geosystems*, **10**, 9.
- Tarantola, A., 1987, *Inverse problem theory. Methods for data fitting and model parameter estimation*: Amsterdam: Elsevier, 1987.
- Tatsumi, Y., H. Shukuno, K. Tani, N. Takahashi, S. Kodaira, and T. Kogiso, 2008, Structure and growth of the Izu-Bonin-Mariana arc crust: 2. Role of crust-mantle transformation and the transparent Moho in arc crust evolution: *Journal of Geophysical Research (Solid Earth)*, **113**, 2203.
- Tichelaar, B. W., and L. J. Ruff, 1993, Depth of seismic coupling along subduction zones: *Journal of Geophysical Research*, **98**, 2017–2037.
- Toomey, D. R., S. C. Solomon, and G. M. Purdy, 1994, Tomographic imaging of the

- shallow crustal structure of the East Pacific Rise at 9 deg 30 min N: *Journal of Geophysical Research*, **99**, 24135.
- von Huene, R., and C. R. Ranero, 2009, *in* *Convergent Margin Structure in High-Quality Geophysical Images and Current Kinematic and Dynamic Models*: Springer, 137.
- Von Huene, R., and D. W. Scholl, 1991, Observations at convergent margins concerning sediment subduction, subduction erosion, and the growth of continental crust: *Reviews of Geophysics*, **29**, 279–316.
- Wadge, G., and J. B. Shepherd, 1984, Segmentation of the Lesser Antilles subduction zone: *Earth and Planetary Science Letters*, **71**, 297–304.
- Waite, W. F., J. C. Santamarina, D. D. Cortes, B. Dugan, D. N. Espinoza, J. Germaine, J. Jang, J. W. Jung, T. J. Kneafsey, H. Shin, K. Soga, W. J. Winters, and T. Yun, 2009, Physical properties of hydrate-bearing sediments: *Reviews of Geophysics*, **47**, G4003+.
- Wang, K., and Y. Hu, 2006, Accretionary prisms in subduction earthquake cycles: The theory of dynamic Coulomb wedge: *Journal of Geophysical Research (Solid Earth)*, **111**, 6410.
- Wang, W., and D. M. Davis, 1996, Sandbox model simulation of forearc evolution and noncritical wedges: *Journal of Geophysical Research*, **101**, 11329–11340.
- Weber, J. C., T. H. Dixon, C. Demets, W. B. Ambeh, P. Jansma, G. Mattioli, J. Saleh, G. Sella, R. Bilham, and O. Pérez, 2001, GPS estimate of relative motion between the Caribbean and South American plates, and geologic implications for Trinidad and Venezuela: *Geology*, **29**, 75.
- Weinzierl, W., and H. Kopp, 2010, Statistical Separation Strategy to Analyze Velocity Structure Obtained by Seismic Tomography: *Geophysics*. (in press).
- Wells, D. L., and K. J. Coppersmith, 1994, New Empirical Relationships among Magnitude, Rupture Length, Rupture Width, Rupture Area, and Surface Displacements: *Bulletin of the Seismological Society of America*, **84**, 974–1002.
- Westbrook, G. K., 1975, The Structure of the Crust and Upper Mantle in the Region of Barbados and the Lesser Antilles: *Geophysical Journal International*, **43**, 201–237.

- Westbrook, G. K., 1982, The Barbados Ridge Complex: Tectonics of a mature forearc system. In: J.K. Leggett (Editor), Trench-forearc geology: sedimentary and tectonics on modern and active ancient plate margins: Geological Society of London Special Publication.
- Westbrook, G. K., J. W. Ladd, P. Buhl, N. Bangs, and G. J. Tiley, 1988, Cross section of an accretionary wedge: Barbados Ridge complex: *Geology*, **16**, 631.
- Westbrook, G. K., M. J. Smith, J. H. Peacock, and M. J. Poulter, 1982, Extensive underthrusting of undeformed sediment beneath the accretionary complex of the Lesser Antilles subduction zone: *Nature*, **300**, 625–628.
- Zelt, C. A., K. Sain, J. V. Naumenko, and D. S. Sawyer, 2003, Assessment of crustal velocity models using seismic refraction and reflection tomography: *Geophysical Journal International*, **153**, 609–626.
- Zelt, C. A., and R. B. Smith, 1992, Seismic travelttime inversion for 2-D crustal velocity structure: *Geophysical Journal International*, **108**, 16–34.

Acknowledgements

First and foremost I am very grateful to Prof. Dr. Heidrun Kopp and Prof. Dr. Ernst Flueh for their continuous support and advice during the last few years. Thank you for the discussions, advice and freedom to look beyond the reasonable.

I am very grateful for the assistance and guidance from Cord Papenberg, Anne Krabbenhöft and Dirk Kläschen in every aspect of the work during the last few years. Thank you for everything.

Many thanks to Martin Scherwath and Lars Planert for their advice during modeling and helpful discussions. Thank you for the help on obtaining the final results.

I would like to thank my entire family for their support during the last few years. Thank you for your love and example.

Many thanks to the participants of RV 'Maria S. Merian' Cruise 04-2, scientists and crew, for the acquisition and pre-processing of the data.

Special thanks to all members of the Geodynamics Department for their friendly assistance and the kind atmosphere within the department.

Erklärung

Hiermit erkläre ich, dass die von mir für das Promotionsverfahren vorgelegte Abhandlung 'Crustal Structure of the Central Lesser Antilles Island Arc: Seismic Near-Vertical and Wide-Angle Profiling', abgesehen von der Beratung der Betreuer nach Inhalt und Form, meine eigene Arbeit ist. Bisher ist die Arbeit noch nicht an anderer Stelle im Rahmen eines Prüfungsverfahrens vorgelegt worden.

Wolfgang Weinzierl

Curriculum Vitae

Personal details:

Name: Wolfgang Weinzierl
Date of Birth: 12.10.1978
Place of Birth: Berlin
Citizenship: German
Address: Hugo-Vogel Str. 47, 14109 Berlin
Email: wweinzierl@ifm-geomar.de

Doctorate:

Since January 2007 PhD student at IFM-GEOMAR, Kiel

Education:

October 2006: German Diplom (equivalent MSc) in Physics
2003 - 2006: Studies of Physics at the Technical University Munich
2002 - 2003: Studies of Physics at the University of North Carolina, Chapel Hill, USA
1998 - 2002: Studies of Physics at the Technical University Berlin
1998: Abitur
1985 - 1998: John-F.-Kennedy School (Gymnasium), Berlin